# Temporal and spatial variation in major ion chemistry and source identification of inorganic aerosols in northern Zhejiang Province, China

Jing-Sha Xu [a,b], Meng-Xia Xu [b], Colin Snape [c], Jun He [a,b,d,e,*], Hong-Hui Xu [f,#], Dong-Sheng Ji [g], Cheng-Jun Wang [h], Huan Yu [i], Hang Xiao [j,k], Yu-Jun Jiang [f], Bing Qi [l], Rong-Guang Du [l]

[a] *International Doctoral Innovation Centre, University of Nottingham Ningbo China, Ningbo, PR China*

[b] *Department of Chemical and Environmental Engineering, University of Nottingham Ningbo China, Ningbo, PR China*

[c] *Faculty of Engineering, University of Nottingham, University Park, Nottingham NG7 2RD, UK*

[d] *Centre for Sustainable Energy Technologies, University of Nottingham Ningbo China, Ningbo, PR China*

[e] *Jiangsu Collaborative Innovation Center of Atmospheric Environment and Equipment Technology (CICAEET), Nanjing University of Information Science & Technology, Jiangsu Key Laboratory of Atmospheric Environment Monitoring and Pollution Control (AEMPC)，Nanjing, PR China*

[f] *Zhejiang Meteorological Science Institute, Hangzhou, PR China*

[g] *State Key Laboratory of Atmospheric Boundary Layer Physics and Atmospheric Chemistry, Institute of Atmospheric Physics, Chinese Academy of Sciences, Beijing, PR China*

[h] *College of Chemistry and Materials Engineering, Wenzhou University, Wenzhou, PR China*

[i] *School of Environmental Science and Engineering, Nanjing University of Information Science and Technology, Nanjing, PR China*

[j] *Hazardous Air Pollutants Lab, Institute of Urban Environment, Chinese Academy of Sciences, Xiamen, PR China*

[k] *Ningbo Urban Environment Observation and Research Station-NUEORS, Chinese Academy of Sciences, Ningbo, PR China*

[l] *Hangzhou Meteorological Bureau, Hangzhou, PR China*

* Corresponding author, email: jun.he@nottingham.edu.cn

[#] Corresponding author, email: forsnow@126.com

## Abstract

To investigate the seasonal and spatial variations of ion chemistry on fine particles in northern Zhejiang Province (NZP), China, a year-long field study was carried out at 4 representative sites (2 urban, 1 suburb and 1 rural sites) in both Hangzhou and Ningbo cities from November 2014 to November 2015. Twelve water soluble inorganic ions (WSII) have been characterized in this study. In NZP, the annual averaged $PM_{2.5}$ concentration was 66.2 ± 37.7 μg $m^{-3}$ and urban sites were observed with more severe $PM_{2.5}$ pollution than the suburban and rural sites; the annual averaged total WSII concentration was 29.1 ± 19.9 μg $m^{-3}$, dominated by $SO_4^{2-}$ (10.3 μg $m^{-3}$), $NO_3^-$ (8.9 μg $m^{-3}$), $NH_4^+$ (6.6 μg $m^{-3}$), $Cl^-$ (1.3 μg $m^{-3}$) and $K^+$ (0.7 μg $m^{-3}$). $NH_4^+$ was highly correlated with $NO_3^-$ and $SO_4^{2-}$ (r: 0.8~1.0) throughout the sampling period at 4 sites and the annual averaged molar ratio of $[NH_4^+]/[SO_4^{2-}]$ of 4 sites were all above 3.3, indicating $NH_4^+$ existed predominantly as $(NH_4)_2SO_4$, $NH_4HSO_4$ and $NH_4NO_3$ in aerosols, which was also the predominant neutralizing cation with the highest neutralization factor (NF). The seasonal patterns of SOR and NOR values were opposite to each other, which seemed influenced by seasonal weather conditions and inter-relationships of $SO_2$ – $SO_4^{2-}$ and $NO_2$ – $NO_3^-$ transformations. Principal component analysis (PCA) showed that the predominant sources of WSII in NZP were industrial emissions, biomass burning, and secondary inorganic aerosols; in addition, transboundary transport of polluted aerosols also contributed based on air mass backward trajectory.



## Keywords

Northern Zhejiang Province, $PM_{2.5}$, inorganic ions, temporal and spatial variability, PCA

## 1. Introduction

Atmospheric aerosols, especially fine particles (aerodynamic diameter of ≤ 2.5 μm, $PM_{2.5}$), comprising a complex mixture of suspended solid particles and liquid droplets, have received a lot of attention over the recent decades due to their important roles in affecting ecology, climate change, visibility and public health, such as respiratory diseases, cardiopulmonary mortality and lung cancer (Pope et al., 2002; Pope and Dockery, 2006; Fang et al., 2011; He et al., 2011; Xu et al., 2016a). In terms of the sources and formation processes, they are basically classified as primary and secondary aerosols; the former are emitted directly from various sources; while the latter are formed through gas-particle transformation. For example, gaseous $SO_2$ and $NO_2$ emitted mostly from coal-fired power plants and vehicles can be oxidized and converted to $SO_4^{2-}$ and $NO_3^-$ in the atmosphere through heterogeneous and homogeneous reactions (Kang et al., 2010; Lin et al., 2009). Then these inorganic species can be converted to secondary aerosol particles such as $(NH_4)_2SO_4$, $NH_4HSO_4$, and $NH_4NO_3$ through the neutralization reactions with $NH_4^+$, which is originated from gas-phase $NH_3$. It is reported secondary inorganic aerosols (sulfate, nitrate and ammonium (SNA)) are one of the most significant contributors to particulate matters (Waldman et al., 1991; He and Balasubramanian, 2008), accounting for one third or more of fine particles (Meng et al., 2016; Tsai and Chen, 2006; Wang et al., 2006); and they are also reported to be one of the most important factors leading to visibility impairment (Kang et al., 2004; Tian et al., 2014). Their formation greatly depends on the characteristics of pre-existing aerosols, occurrence levels of the gaseous precursors, relative humidity (RH) and atmospheric oxidants etc. (Baek et al., 2004; Deng et al., 2015; Pathak et al., 2009).

In China, due to the significantly decreasing air quality during recent decades across the country, the pollution characteristics of aerosols have been widely studied. Among various

components of atmospheric aerosols, water-soluble components are of great interest in urban atmosphere due to their impact on controlling the aerosol acidity and environmental acidification (Deng et al., 2015). The earliest studies on WSII can be traced back to 1990s in China (Waldman et al., 1991), and after that a number of researches have been conducted in many cities to investigate the characteristics of water-soluble inorganic ions, such as Xiamen (Zhao et al., 2011), Handan (Meng et al., 2016), Guangzhou (Hu et al., 2008), Jinan (Gao et al., 2011) and Beijing (Hu et al., 2014; Huang et al., 2016), etc. Yangtze River Delta (YRD) is one of the largest city-clusters and economically well-developed regions in China, and WSII characteristics of severe aerosol pollution in this region have also been reported to some extent. In a western city of YRD-Nanjing, Wang et al. (2016b) studied the seasonal and diurnal variations and sources of water-soluble inorganic ions based on one-year online measurement data. Qiao et al. (2015) investigated the seasonal variation of WSII in $PM_1$ and their effects on haze episodes in Shanghai. Hua et al. (2015) studied the ion characteristics of $PM_{2.5}$ during a severe haze episode by a joint field observations at five cities in YRD and the source apportionment indicated that $PM_{2.5}$ was predominantly from secondary pollutants and primary emissions of vehicles and biomass burning. In an offshore site at east coastal line of Jiangsu Province, Kong et al. (2014) investigated the ion chemistry including the ion mass concentration, ion balance and sea salt contributions of size-segregated aerosols in autumn 2012 and found the sea salt contribution could be ignored despite its geographical closeness to the East China Sea. Most of the previous studies of ionic chemistry in fine aerosols in this region have been either based on a particular haze episode or a particular sampling site, which may not represent the seasonal ion pollution characteristics of the YRD region well. Due to the absence of long-term observation of atmospheric inorganic ions in this region, Wang et al. (2015a) investigated the seasonal

variations and sources of water-soluble inorganic ions in size-fractionated aerosols of 5 urban sites in YRD, but their data lacked the comparisons among the ion chemistry in urban, suburban and rural areas in YRD. In this respect, the investigation of the seasonal ion chemistry and sources in fine particles of urban, suburban and rural sites in YRD should be valuable to filling such a gap and gain further knowledge of how ion chemistry in fine particles of various representative sites in this region might differ from one another.

Due to the limited study of WSII on fine aerosols in northern Zhejiang Province (NZP), 12 ionic species ($F^-$, $Cl^-$, $NO_2^-$, $NO_3^-$, $PO_4^{3-}$, $SO_4^{2-}$, $Li^+$, $Na^+$, $NH_4^+$, $K^+$, $Mg^{2+}$, $Ca^{2+}$) from 4 different representative sites in this area located in the southern YRD were investigated, including two urban, one suburban and one rural site. The main objectives of this work were to characterize the temporal and spatial variations of fine aerosols and above mentioned ionic species profiles in NZP, compare the ionic chemistry at sites with different urbanization gradients and explore the potential sources of these fine inorganic aerosols in this region.

## 2. Experimental

### 2.1. Sampling site

In order to investigate the ion chemistry of $PM_{2.5}$ and their possible sources in NZP, different types of representative sampling sites have been selected in both cities of Hangzhou and Ningbo, which are presented in Fig. 1 and briefly introduced as below.

1) The University of Nottingham Ningbo, China (UNNC; suburban site; 29.80°N, 121.56°E) is located at the University Park in the south of Ningbo city, less than 10km away from the central business district (CBD). It can be characterized as an intermediate transition zone which is affected by the pollution from both urban and rural anthropogenic activities.

2) Ningbo Meteorological Bureau (NMB; urban site; 29.86°N, 121.52°E) is located by the side of a main road– Qixiang Road in Ningbo urban center and adjacent to a high school and residential area. It is also only approximately 1km away from the airport highway elevated bridge and 500m from a provincial highway. Therefore, it is expected to be influenced more by traffic emissions.

3) Lin'an Regional Atmospheric Background Station (LRABS; rural site; 30.30°N, 119.73°E) , at the outskirt of Lin'an county within Hangzhou municipality, is a background monitoring station for the World Meteorological Organization (WMO) global atmospheric observation network. It is surrounded by agricultural fields and woods, and less affected by urban, industrial and vehicular emissions.

4) Hangzhou Meteorological Bureau (HMB; urban site; 30.22°N, 120.17°E) is one of the national atmospheric and meteorological monitoring stations in China. It is located at the urban center of a densely populated city– Hangzhou, and close to a few heavy traffic roads with distance around 200m.

## 2.2. Sample collection

The collection of $PM_{2.5}$ was started simultaneously at 9 AM (1 UTC) at four above mentioned sites every 6 days from 12 November 2014 to 12 November 2015. The 24-hour sampling was conducted by medium volume $PM_{2.5}$ samplers (Model: TH-150CIII, Tianhong Instrument CO., Ltd. Wuhan, China), operating at a flow rate of 80 L $min^{-1}$ and $PM_{2.5}$ aerosols were captured on 90 mm quartz fiber filters (QMA, Whatman, UK). All filters were pre-baked in muffle furnace for 5 hours at 550°C prior to any other treatments or usage. Blank samples were obtained monthly at four sites.

## 2.3. Acquisition of $PM_{2.5}$ mass, meteorological data and air mass backward trajectories

Prior to any gravimetric measurement, filters were equilibrated in a micro-balance room with constant temperature (22°C ± 1°C) and relative humidity (30% ± 5%) for 24h before and after the sampling events. The $PM_{2.5}$ mass on 90mm quartz fiber filters were measured by an ultra-microbalance (Model: SE2-F, Sartorius, precision 0.1 μg). After that, filters were wrapped in prebaked aluminum foil and stored in refrigerator under -20°C until analysis.

Meteorological data (wind speed, precipitation, temperature and relative humidity) and concentrations of gaseous pollutants ($SO_2$, $NO_2$, $O_3$) applied in this study were obtained from the corresponding local air quality monitoring stations closest to each sampling site (less than 500m distance) during the same aerosol sampling periods.

The air mass backward trajectories were computed from archived global data assimilation system (GDAS1, 2006-present) meteorological data. 96 hours air mass backward trajectories were started at 9:00 AM local time (1 UTC) with 6 hours intervals at a height of 500 m above ground level (AGL) on each sampling day and calculated separately for each sampling site. Achieved trajectories were then clustered by season using the air resources laboratory (ARL) of National Ocean and Atmospheric Administration (NOAA) Hybrid Single-Particle Integrated Trajectory (HYSPLIT 4.9) model (Draxler, 2013; Rolph, 2013), and those trajectories with similar sources were merged. Clusters can reduce errors that might be related to a single trajectory and indicate more accurate origins of those pollutants.

## 2.4. Ionic analysis

One eighth 90mm quartz fiber filters were used for ion analysis, which were extracted ultrasonically using 20 mL of deionized water for 30 min, filtered with the 0.45μm PTFE microporous membrane and stored in a refrigerator at 4°C until chemical analysis within two

weeks. In total, 6 anions ($F^-$, $Cl^-$, $NO_2^-$, $NO_3^-$, $PO_4^{3-}$, $SO_4^{2-}$) and 6 cations ($Li^+$, $Na^+$, $NH_4^+$, $K^+$, $Mg^{2+}$, $Ca^{2+}$) were investigated by Ion Chromatograph (ICS-1600, Dionex, USA). Detailed information about the detection system and methods could be found elsewhere (Xu et al., 2016b). Ion concentrations were calculated through the external calibration ($r^2 \geq 0.99$) with authentic standards purchased from Sigma-Aldrich and corrected by subtracting blank values obtained from field blank samples.

## 3. Results and discussion

### 3.1. Air mass backward trajectory analysis

The air mass backward trajectories are very useful to identify the source origins of the particulate pollutants measured at the sampling sites. Fig. 2 shows the clusters of air mass backward trajectories during each season at different representative sampling sites of NCP, which exhibited distinctive seasonal variations.

In winter, clusters at four sites were very similar to each other in this region; 75%-97% of the air masses were coming through northwest and north China before arriving at the sampling sites and part of them were originated from Russia and Kazakhstan. In spring, 13%-37% were originated from northwestern Asia; at UNNC and NMB, 20%-30% were from northwestern China and the rest were from either a mixed oceanic and terrestrial source or local origins in YRD; at LRABS and HMB, around 50% of air masses were from central China and local YRD region, respectively. In summer, 45%-64% of the air masses were originated from Chinese Bohai Sea and Pacific Ocean and another part was from South China Sea and passing through southern China to reach the studied sites with both oceanic and terrestrial source characteristics; the rest 10-29% was from the central China. In autumn, the clusters at UNNC and NMB showed similar origins due to their geographical closeness to each other; approximately 40% of the trajectories

were originated from Russia and Inner Mongolia and the rest were from oceanic origin; at LRABS and HMB, around 20% of trajectories were coming from north China, the rest were with mixed origins of both ocean and land, among of which 10~20% were transported through south China to sampling sites.

### 3.2. Spatial and temporal variability of meteorological conditions and $PM_{2.5}$ concentrations in NZP

Continuous hourly measured meteorological data were converted to give daily averaged values from 9 AM on the sampling day to the same time next day. The seasonal mean meteorological parameters (calculated as the daily average of sampling days during each season), including wind speed (m $s^{-1}$), precipitation (mm), temperature (°C) and relative humidity (RH, %) at four sampling sites throughout the sampling campaign are summarized in Table 1.

The seasonal averaged temperature and RH at four sampling sites followed the same pattern: Summer > Autumn > Spring > Winter. This is most likely due to the typical marine monsoon subtropical climate in NZP of YRD region, thus all sampling sites in this region are featuring cool dry winters and hot humid summers (Haas and Ban, 2014). The seasonal mean highest temperature in NZP was 26.7°C during summer and the lowest was 6.3°C during winter. Winter was also recorded as the driest season with RH of 64.1% and summer was recognized as the most humid season with RH of 77.8%. The wind speeds of winter, spring and summer were very similar, but that in autumn was obviously lower than the other seasons, implying a more stagnant meteorological condition and weaker advection for dispersion.

The annual average $PM_{2.5}$ concentration in this region (calculated as the average of $PM_{2.5}$ at four sampling sites) was 66.2 ± 37.7 μg $m^{-3}$, which is nearly twice the National Ambient Air Quality Standards of China– Grade II (35 μg $m^{-3}$ for annual $PM_{2.5}$ concentration), applicable to

residential, commercial, industrial and rural areas (MEP, 2012). To compare this result with those in other cities of YRD, it is higher than the 3-year average $PM_{2.5}$ concentration (47 μg $m^{-3}$) measured in Shanghai (Wang et al., 2016c), but comparable with the annual $PM_{2.5}$ occurrence levels in Hangzhou (64 ± 47 μg $m^{-3}$) and Nanjing (75 ± 50 μg $m^{-3}$) (Wang et al., 2014). The annual average concentration of $PM_{2.5}$ at four sites ranked as: UNNC (51.2 ± 29.1 μg $m^{-3}$) < LRABS (66.3 ± 36.6 μg $m^{-3}$) < NMB (70.4 ± 40.6 μg $m^{-3}$) < HMB (80.0 ± 39.6 μg $m^{-3}$). Clearly, the annual average $PM_{2.5}$ concentrations in urban sites (NMB & HMB) were higher than the other two suburban and rural sites (UNNC & LRABS), possibly indicating stronger anthropogenic sources could contribute more to the higher occurrence levels of fine aerosol particles in urban areas. Among four sites, UNNC was observed with the lowest annual $PM_{2.5}$ concentration and the highest average wind speed throughout the sampling period. Besides the reasons such as less local emission impact that could be beneficial to the lower occurrence of $PM_{2.5}$ levels at this site, the easier dispersion of aerosol by the stronger wind speed and smoother terrain feature surrounding the sampling site could also be one of them.

The averaged seasonal variations of $PM_{2.5}$ concentrations at two urban sites (NMB & HMB) showed the following pattern: Winter > Spring > Autumn > Summer, which is consistent with that in an urban site of Shanghai (Wang et al., 2016c); while the occurrence levels of $PM_{2.5}$ in suburban and rural sites (UNNC & LRABS) showed slightly different: Winter > Autumn > Spring > Summer, the same as that observed in a western downtown sampling area in Nanjing of YRD (Li et al., 2015).

Among four seasons, the highest average $PM_{2.5}$ concentration was observed in winter while the lowest in summer. Heavy particle pollution in winter could be the synergetic effect of increased emission from fuel burning and accumulation of pollutants under stagnant weather

conditions. Lower temperature in winter would lead to the increasing consumption of fuel, such as biomass burning in rural areas and coal combustion in power plants, to meet the increased energy demands for domestic house heating (Behera et al., 2015), resulting in more intensive exhaust of air pollutants (Han et al., 2016). Meanwhile, these air pollutants would accumulate under more calm and static atmospheric environment in winter as this season in this region is normally characteristic of low wind speed, weak solar radiation and strong surface inversion, which would lead to low planetary boundary layer (PBL) height and poor air dispersion (Behera et al., 2015; Seidel et al., 2010). While in summer, wind mostly blows from the East China Sea where less polluted air mass is transported to YRD; in addition, higher mixing layer during hot summer could induce stronger vertical diffusion and dispersion of air pollutants.

It is noteworthy that the seasonal averaged $PM_{2.5}$ concentrations in autumn were lower than those in spring of two urban sites (NMB and HMB), but they were opposite at the other two suburb and rural sites. These findings could be the result of various wet precipitation rates during the different seasons and stronger precipitation favored to increase the scavenging of aerosols. In addition, at suburban and rural sites, more open burning events for land clearing tend to occur during autumn harvest season, mainly in October and November (Yin et al., 2017). Therefore, at UNNC and LRABS, more emissions from biomass burning were expected to contribute to the higher $PM_{2.5}$ concentrations in autumn than in spring.

### 3.3. Characteristics of water-soluble inorganic ions (WSII)

#### 3.3.1. Annual occurrence level of total WSII

The annual average concentration of total WSII in NZP was 29.1 ± 19.9 μg $m^{-3}$, constituting 44.0% of the annual average $PM_{2.5}$ concentration. Sulfate, nitrate and ammonium (SNA) ranked as the top three ions with highest concentrations in this study, and the sum of them was 25.6 ±

253 18.4 μg $m^{-3}$, accounting for 88.0% of total WSII and 38.7% of $PM_{2.5}$ concentration in this region,
254 respectively.

255 In order to better understand the fine aerosol pollution in YRD, intra- and inter-city
256 comparisons have been conducted as presented in Table 2 and other polluted areas in China
257 including North China Plain (NCP), Northwest China (NWC) and Pearl River Delta (PRD).

258 Cities in NCP such as Handan, Hefei and Tianjin were observed with much higher $PM_{2.5}$ and
259 total WSII concentrations, but the mass ratio of WSII in $PM_{2.5}$ is comparable to those found in
260 this study (Deng et al., 2015; Meng et al., 2016; Zhou et al., 2016). In addition to the effects of
261 stagnant meteorological conditions leading to high accumulation or trans-boundary transport of
262 pollutants originated from other regions, it seems that the aerosol pollution in different regions
263 also have its own characteristics. Higher particle pollution level in NCP is most likely due to the
264 numerous anthropogenic emissions from heavy industries and strong traffic emissions in this
265 region, as a result of its rapid population growth and economic development in past few decades
266 (Ran et al., 2016). Cities like Xi'an and Weinan in NWC were also observed with higher aerosol
267 concentrations, but the one in Xi'an had a relatively lower WSII/$PM_{2.5}$ ratio compared to this
268 study (Niu et al., 2016; Zhang et al., 2011), which might be due to its higher mineral dust
269 contribution as it occurs frequently in this area (Zhang et al., 2011). The occurrence levels of fine
270 aerosols in urban PRD area seem very comparable to those in this study (Tao et al., 2009; Zhou
271 et al., 2016). In Shanghai a two-year (2012-2013) sampling campaign found out that the average
272 $PM_{2.5}$ concentration was lower than those reported in other cities in YRD, but WSII/$PM_{2.5}$ ratio
273 was over 60% indicating a strong contribution of secondary inorganic ions to fine aerosols in this
274 urban area (Wang et al., 2016c).

3.3.2. Spatial and temporal variability of WSII in northern Zhejiang Province

The annual total WSII concentrations at four sampling sites followed such an order: UNNC ($21.0 \pm 10.8$ μg $m^{-3}$) < NMB ($26.7 \pm 18.8$ μg $m^{-3}$) < LRABS ($29.6 \pm 18.2$ μg $m^{-3}$) < HMB ($41.3 \pm 25.5$ μg $m^{-3}$), contributed to 38.6% ~ 49.2% of $PM_{2.5}$, as shown in Table 2. Similar to the occurrence levels of $PM_{2.5}$ and WSII, SNA exhibited much higher concentrations in NCP and NWC than those in this study, which however seemed comparable to the reported values in YRD and PRD. The annual SNA concentration at UNNC, the suburban site of Ningbo, was 17.4 μg $m^{-3}$, accounting for 81.9% of total WSII concentration and 35.8% of $PM_{2.5}$; while at NMB, the urban site of Ningbo, higher annual SNA concentration of 23.0 μg $m^{-3}$ was observed with higher mass ratio of 83.3% in total WSII but lower proportion of 32.9% in $PM_{2.5}$. Higher annual SNA concentrations of 27.2 μg $m^{-3}$ (90.5% of total WSII concentration and 40.5% of $PM_{2.5}$) and 37.0 μg $m^{-3}$ (88.8% of total WSII concentration and 44.5% of $PM_{2.5}$) were observed at LRABS and HMB in Hangzhou, respectively, suggesting the secondary aerosol formations at both sites were more significant than Ningbo.

Table 3 illustrates the seasonal and annual averaged WSII concentrations at four sampling sites. Among the investigated ions at all sites, $NH_4^+$, $NO_3^-$, $SO_4^{2-}$ and $Cl^-$ were of predominance and the first three are known to be the dominant secondary particles with their abundances mainly dependent on the concentrations of their precursor gases and transformation rates. As shown in Table 3, winter was observed with the highest ionic concentrations while summer was observed with the lowest. The concentrations of both ammonium and nitrate in winter were 2~6 times higher than those in summer. This could be related to the low temperature in winter that favors a conversion from nitric acid and ammonia gases to the particulate ammonium nitrate and also that most nitrate would prefer to be gaseous at temperature higher than 30ºC (Deng et al.,

298 2015). The seasonal variation of nitrate concentration could also be attributed to the seasonality
299 of $NO_x$ emission (Li and Han, 2016). It is known that both HCl and $SO_2$ are the typical pollutants
300 emitted from coal combustion (Xue et al., 2016); hence, the highest abundance of both sulfate
301 and chloride in winter could be likely due to the increased coal consumption during heating
302 period combined with poor dispersion (He et al., 2001). In addition to the local emissions, during
303 winter in YRD, the prevalent north or northwest winds can bring atmospheric pollutants from
304 NCP, where more consumption of coal for domestic heating also occurs in this season (Wang et
305 al., 2016c), to the sampling sites in this study via long-range transport, which was supported by
306 air mass backward trajectory analysis in Section 3.1 that 75%-97% of the air masses were
307 coming through northwest and north China before arriving at the sampling sites.

308 Apart from $NH_4^+$, $Cl^-$, $NO_3^-$ and $SO_4^{2-}$, the concentration of $K^+$ was the highest among the rest
309 ions. The highest concentration of $K^+$ occurred in winter as well, it is around 2~4 times higher
310 than summer at four sites. As it is predominantly generated from biomass burning, such as wood,
311 grass and crop straw burning (Xu et al., 2016b), suggesting biomass burning is an important
312 contributor to the fine particles in the NZP, which can be supported by the high level of non-sea
313 salt (nss) $K^+$ during winter (1.0 μg $m^{-3}$) and spring (0.9 μg $m^{-3}$) in a rural site- LRABS.

314 3.3.3. Aerosol acidity

315 (1) Ion balance

316 Water-soluble inorganic ions play important roles in controlling the aerosol acidity and
317 environmental acidification. Therefore, the aerosol acidity is also investigated in this study by
318 ion balance, which is determined by both anion equivalence (AE) and cation equivalence (CE),
319 calculated by following equations:

320 $$AE = F^-/19 + Cl^-/35.5 + NO_2^-/46 + Br^-/80 + NO_3^-/62 + PO_4^{3-}/31.7 + SO_4^{2-}/48 \quad (1)$$

$$CE = Li^+/7 + Na^+/23 + NH_4^+/18 + K^+/39 + Mg^{2+}/12 + Ca^{2+}/20 \quad (2)$$

Where, $F^-$, $Cl^-$, $NO_2^-$, $NO_3^-$, $PO_4^{3-}$, $SO_4^{2-}$, $Li^+$, $Na^+$, $NH_4^+$, $K^+$, $Mg^{2+}$, and $Ca^{2+}$ refer to their mass concentrations (μg $m^{-3}$). Through calculations by the above equations, the anion and cation concentrations (μg $m^{-3}$) were converted into their corresponding micro-equivalents (μ mol $m^{-3}$) and the relationships between AE and CE in four seasons of the sampling sites are plotted in Fig. 3.

As shown in Fig. 3, good correlations and very small intercepts between AE and CE were found in 4 seasons; therefore, the anion/cation equivalent ratios (AE/CE) were defined as the slopes of linear regressions in this study. At 4 sites, the correlation coefficients of AE and CE were in the range of 0.77~0.99, similar to the results in another study of YRD (0.72~0.94) (Wang et al., 2015a). At UNNC and HMB, the AE/CE ratios in four seasons were mostly above 1.0, except the ratio close to 1 in the summer of UNNC. These results indicated a deficiency in cations of $PM_{2.5}$ samples in UNNC and HMB, anions were not fully neutralized and caused acidic nature of fine particles at these two sites. When using the equivalent ratio of $[NH_4^+]/[NO_3^-+SO_4^{2-}]$ to evaluate the aerosol acidity (Wang et al., 2016a), the ratio at HMB was 0.99, indicating a good neutralization relationship between the major secondary species at this site during the sampling period. At UNNC, the annual averaged equivalent ratio of $[NH_4^+]/[NO_3^-+SO_4^{2-}]$ was only 0.89, while the annual averaged equivalent ratio of $[NH_4^+ + Ca^{2+}]/[NO_3^- + SO_4^{2-}]$ of UNNC could be up to 0.98, suggesting $Ca^{2+}$ might be another main cation affecting the neutralization of $NO_3^-$ and $SO_4^{2-}$ . This could be explained by the fact that a number of construction sites existed around UNNC during this sampling campaign, which might be the dominant sources of $Ca^{2+}$ at this site showing strong influence on the ionic chemistry here.

In LRABS, during winter and spring, it had lower AE/CE value (<1) and the seasonal averaged equivalent ratio of $[NH_4^+]/ [NO_3^-+SO_4^{2-}]$ of winter and spring were 1.13 and 1.36, respectively, implying the aerosol samples during these two seasons were alkaline, probably due to the increased biomass burning in winter and more usage of ammonia containing fertilizer in spring for cultivation at this rural site (Whitburn et al., 2015). The aerosol collected in autumn at Lin'an had shown higher AE/CE ratio (=1.09), indicating these aerosols were more acidic, which could be attributed to the higher occurrence level of $NO_3^-$ in autumn , which was 2.8 times that during summer when ammonium nitrate is more easily volatilized as mentioned before. The AE/CE ratio during summer at Lin'an was close to 1 and the averaged equivalent ratio of $[NH_4^+]/ [NO_3^-+SO_4^{2-}]$ was 0.95, indicating anions and cation maintained a good neutralization relationship.

The AE/CE slope of the linear regression for NMB were all lower than 0.9 in the whole sampling campaign; since most of the anions were analyzed but not the carbonate and bicarbonate due to the limitation of the Ion Chromatogram (IC) method, the anion deficits in aerosol samples of NMB could be partially attributed to the absence of both ions (Meng et al., 2016). The annual averaged equivalent ratio of $[NH_4^+]/ [NO_3^-+SO_4^{2-}]$ of NMB was 1.11, also suggesting $NH_4^+$ was over-sufficient to neutralize $NO_3^-$ and $SO_4^{2-}$. The excess of $NH_4^+$ could be associated with anions like chloride and carbonate. Moreover, since NMB is located by the side of a main road and near a couple of highways, it is expected to be influenced heavily by traffic emissions, an important source of urban $NH_3$ derived from urea used in the selective catalytic reduction (SCR) in vehicular engines (Pan et al., 2016), which seems supported by the higher annual concentration of $NH_4^+$ at urban site NMB (6.6 μg $m^{-3}$) than suburban site UNNC (3.9 μg $m^{-3}$) in Ningbo.

(2) Neutralization Factors (NF)

In order to further find out the significance of each cation in neutralizing aerosol acidity, the neutralization capacities of major cations (nss-$Ca^{2+}$, $Mg^{2+}$, nss-$K^{+}$ and $NH_4^{+}$) were individually estimated by applying the Neutralization Factors (NFs). $SO_4^{2-}$ and $NO_3^{-}$ were considered as the dominant acidifying anions. $Na^{+}$ and $Cl^{-}$ were considered negligible in past few studies for calculation of NF, as they existed mostly in the form of neutral sea salt (Safai et al., 2010; Satsangi et al., 2013). However, in this study, poor correlation of $Na^{+}$ and $Cl^{-}$ ($r^2 < 0.5$) were found at all four sites, suggesting possible different origins of $Cl^{-}$. Moreover, the $Na^{+}$/ $Cl^{-}$ equivalent ratios of UNNC, NMB, LRABS and HMB were 0.47, 0.53, 0.91 and 0.51, respectively, lower than that in seawater (1.1) (Xu et al., 2014), implying $Cl^{-}$ could also have other sources such as coal combustion and waste incineration in addition to sea salt (Xue et al., 2016). LRABS had the highest $Na^{+}$/ $Cl^{-}$ equivalent ratio (0.91) and lowest $Cl^{-}$/ $PM_{2.5}$ mass ratio (0.9%) among four sites (HMB: 1.8%; NMB: 2.2%; UNNC: 2.9%), suggesting relatively more marine effect yet less contribution of other combustion processes at this rural site. Therefore, the role of $Cl^{-}$ in neutralization could not be neglected in this study. As $Na^{+}$ was assumed to be all derived from the ocean (Kong et al., 2014), and it predominantly existed as NaCl in sea salts (Ueda et al., 2014), hence non-sea salt [$Cl^{-}$] can be calculated by subtracting [$Na^{+}$] from [$Cl^{-}$] and NFs were calculated by Equation (3-6):

$$NF\ (nss-Ca^{2+}) = [nss-Ca^{2+}]/([nss-SO_4^{2-}] + 2[NO_3^{-}] + 2[Cl^{-}] - 2[Na^{+}]) \quad (3)$$

$$NF\ (Mg^{2+}) = [Mg^{2+}]/([nss-SO_4^{2-}] + 2[NO_3^{-}] + 2[Cl^{-}] - 2[Na^{+}]) \quad (4)$$

$$NF\ (nss-K^{+}) = [nss-K^{+}]/(2[nss-SO_4^{2-}] + [NO_3^{-}] + [Cl^{-}] - [Na^{+}]) \quad (5)$$

$$NF\ (NH_4^{+}) = [NH_4^{+}]/(2[nss-SO_4^{2-}] + [NO_3^{-}] + [Cl^{-}] - [Na^{+}]) \quad (6)$$

388 [X] represents the molar concentration of ions, and nss-$SO_4^{2-}$, nss-$K^+$ and nss-$Ca^{2+}$ were
389 estimated in section 3.4.1.

390 Fig. 4 depicts the NFs of nss-$Ca^{2+}$, $Mg^{2+}$, nss-$K^+$ and $NH_4^+$ in $PM_{2.5}$ at 4 sites of northern
391 Zhejiang Province. As expected, $NH_4^+$ was the predominant neutralizing cation with the highest
392 NF, and the average annual NF of $NH_4^+$ at 4 sites were LRABS (1.12) > NMB (1.08) > HMB
393 (0.95) > UNNC (0.83). The annual NF of $NH_4^+$ in LRABS and NMB were above 1, indicating
394 the excess of $NH_4^+$ after neutralizing nss-$SO_4^{2-}$, $NO_3^-$ and $Cl^-$, which might also be explained by
395 those reasons discussed in Section 3.3.3 for part of AE/CE ratios smaller than unity at these two
396 sites. The NF values of nss-$Ca^{2+}$, nss-$K^+$ and $Mg^{2+}$ were lower than 0.2, implying relatively
397 minor impact of these ions in the neutralization of aerosol acidity. On an annual basis, the
398 neutralization capacities of ions in UNNC and NMB ranked as: $NH_4^+$ > nss-$Ca^{2+}$ > nss-$K^+$ >
399 $Mg^{2+}$. Nss-$Ca^{2+}$ was the second dominant neutralizing cation at both sites of Ningbo, possibly
400 due to the strong dust effect from the nearby construction areas and main roads as discussed
401 before. In LRABS, the annual averaged NF of nss-$K^+$ was the second highest after $NH_4^+$, which
402 is reasonable since biomass burning is a common activity in rural area for land clearance and
403 house heating possibly to contribute more nss-$K^+$ to the local atmosphere. In HMB, NFs of nss-
404 $K^+$ during both winter and autumn were the second highest among four cations, possibly due to
405 the enhanced local biomass burning for house heating in winter and open crop residue burning in
406 autumn (Chen et al., 2016). Additionally, as shown in Fig. 2, the majority of air masses reaching
407 HMB were coming through highly polluted NCP, rural site- LRABS (located at the northwest of
408 HMB) and agriculture lands dominated western and northern suburban areas of Hangzhou
409 (Sheng et al., 2017), hence, elevated $K^+$ could be expected at HMB due to medium- and short-
410 range transport.

411 3.4. Ion chemistry and source identification

412 3.4.1. Marine contribution of the aerosol composition

413 As located at the east coast of China, bordering the East China Sea and Yellow Sea, marine
414 effects seemed not to be ignored in this work. Therefore, the non-sea salt (Toledano et al., 2012)
415 contribution to aerosols has been evaluated. $Na^+$ was assumed to be all derived from the sea and
416 non-sea salts were calculated using following equation (Kong et al., 2014):

417 $$nss\text{-}X = X_i - Na^+_i \times (X/Na^+)_{sea} \quad (7)$$

418 where, $X_i$ and $Na^+_i$ represent the ion and $Na^+$ concentration in aerosol samples respectively.
419 $(X/Na^+)_{sea}$ is ratio of ion and $Na^+$ in seawater. The $(X/Na^+)_{sea}$ ratios for $Ca^{2+}$, $K^+$ and $SO_4^{2-}$ are
420 0.0385, 0.037 and 0.2516, respectively, based on the seawater composition (Balasubramanian et
421 al., 2003).

422 Fig. 5 depicts the concentrations of nss-$SO_4^{2-}$, nss-$K^+$, nss-$Ca^{2+}$ and the respective nss-$SO_4^{2-}$
423 /$SO_4^{2-}$, nss-$K^+$/$K^+$ and nss-$Ca^{2+}$/$Ca^{2+}$ ratios. High ratios (≥ 0.86) of nss-$SO_4^{2-}$/$SO_4^{2-}$, nss-$K^+$/$K^+$
424 and nss-$Ca^{2+}$/$Ca^{2+}$ were found at all four sites, indicating minor marine contribution (≤ 14%) to
425 these ions. In LRABS and HMB, the nss-$SO_4^{2-}$/$SO_4^{2-}$ of all seasons was up to 0.99, indicating the
426 marine influence on sulfate concentration is negligible. The trend of nss-$SO_4^{2-}$/$SO_4^{2-}$ during all
427 seasons in UNNC and NMB were quite similar and the ratios in winter, spring and autumn were
428 around 0.98-0.99; while marine source affected UNNC and NMB more in summer with a
429 contribution of non-sea salt to total sulphate up to 97%, which could be attributed to the slightly
430 elevated air mass from the sea compared to the other two sites, as shown in the trajectory clusters
431 of Fig. 2.

432 Nss-$K^+$ has been revealed as a tracer of biomass burning (Chow et al., 2004), the nss-$K^+$
433 concentration in winter were more than twice that in summer and the highest nss-$K^+$/$K^+$ also

occurred in winter at all four sites, indicating the heaviest biomass burning contribution to the high level of fine particles in winter and minimum marine influence while most significant biomass burning impact on $K^+$ during this season. Relatively higher nss-$K^+$ in autumn and spring could also be the result of biomass burning during these two seasons, especially the straw burning during both harvest periods in this region. However, in the summer at UNNC and NMB, more sea salt contribution to $K^+$ with lowest nss-$K^+/K^+$ was observed, possibly due to the stronger air masses transported from oceanic origins in this season. The high value of nss-$Ca^{2+}/Ca^{2+}$ indicate $Ca^{2+}$ was not majorly related to marine origin but more of continental contribution.

3.4.2. Correlations between WSIIs

The correlation between WSII mass concentrations is a good way to investigate the possible sources and associations among various ionic species. Correlation results, shown as the correlation coefficients (r), are provided in Supplemental Table S1-S16.

The secondary species, ammonium sulfate ($(NH_4)_2SO_4$), ammonium bi-sulfate ($NH_4HSO_4$) and ammonium nitrate ($NH_4NO_3$), namely secondary inorganic aerosol (SIA), are generated through both homogeneous and heterogeneous reactions of gaseous precursors ($SO_2$, $NO_2$, $NH_3$). Their formation depends on the availability of their corresponding precursor gases and the atmospheric conditions. It is reported that ammonia would first neutralize with sulphuric acid to form $NH_4HSO_4$ and $(NH_4)_2SO_4$, then the remaining ammonia would react with nitric acid to generate $NH_4NO_3$ (Squizzato et al., 2012). $NH_4^+$ was found out significantly correlated with $NO_3^-$ and $SO_4^{2-}$ throughout the sampling period at 4 sites, and most of their correlation coefficients were in the range of 0.80~0.99; moreover, the annual averaged molar ratio of $[NH_4^+]/[SO_4^{2-}]$ at 4 sites were above 3.3, indicating the coexistence of $(NH_4)HSO_4$, $(NH_4)_2SO_4$

457 and $NH_4NO_3$. Higher correlations between $NH_4^+$ and $SO_4^{2-}$ than $NH_4^+$ and $NO_3^-$ were found in
458 summer at 4 sites, indicating the primary formation of sulfates instead of nitrates during the
459 summer in NZP, which is also supported by the molar ratio of $[NH_4^+]/[SO_4^{2-}]$ with an average of
460 2.2 throughout the summer at all sites.

461 In winter, except the strong correlations between major secondary ionic species, $NO_2^-$ was
462 found to correlate highly with $Mg^{2+}$ (r = 0.80) and $Ca^{2+}$ (r = 0.88) in UNNC (Table S1), implying
463 the major existence of $NO_2^-$ was $Mg(NO_2)_2$ and $Ca(NO_2)_2$. Since it has been reported that $NO_2^-$
464 can be formed through heterogeneous conversion of $NO_2$ on wet particle surface (Wang et al.,
465 2015b), good correlations between $NO_2^-$ and $Mg^{2+}$ and $Ca^{2+}$ could possibly be due to the efficient
466 conversion from $NO_2$ to $NO_2^-$ on these mineral particles. $Mg^{2+}$ and $Ca^{2+}$ was found to correlate
467 well (r = 0.85) in winter at Lin'an (Table S9), likely attributed to their common sources such as
468 soil dust from the surrounding agricultural environment under dry and windy condition during
469 winter (Satsangi et al., 2013). The ratio of $Mg^{2+}$/ $Ca^{2+}$ is 0.34 during winter in Lin'an, higher
470 than 0.12 in sea salt aerosol (Deng et al., 2015), reconfirming sea salt was not a major
471 contributor. As mentioned before, $K^+$ is treated as a tracer for biomass or biofuel emissions,
472 which is observed to correlate well with $PM_{2.5}$ in Lin'an (r = 0.84) (Table S9) and Hangzhou (r =
473 0.88) (Table S13), indicating the significant contributions from biomass burning to the
474 occurrence levels of aerosol at these two sites. Since biomass burning is reported as the second
475 largest emission source of $NH_3$ from land clearing activity (Whitburn et al., 2015), good
476 correlations between $K^+$ and $NH_4^+$ (r=0.80, Table S13) also supported the above statement on
477 contribution of biomass burning to high aerosol concentrations at Hangzhou.

478 In spring at UNNC, $K^+$ and $NH_4^+$ (r = 0.82), $Cl^-$ and $NO_2^-$ (r = 0.87) were also found
479 correlated (Table S2), suggesting their common source like coal combustion and biomass

480 burning (Pei et al., 2016; Whitburn et al., 2015). Even though $Na^+$ and $Cl^-$ correlated very well (r
481 = 0.88), the equivalent ratio of $Na^+/Cl^-$ was only 0.44, much lower than their equivalent ratio in
482 seawater (1.1), suggesting marine source was only one of its major origins and regional soil
483 could also be partially responsible for their tight correlation (Xu et al., 2014). As NOx is also
484 emitted from biomass burning (Chen et al., 2016), good correlations (r = 0.83 and 0.87,
485 respectively, Table S10) between $K^+$ and $NO_3^-$ may imply their common source of biomass
486 burning at NMB and Lin'an. In Hangzhou (Table S14), $Mg^{2+}$ correlated with $Ca^{2+}$ (r = 0.85) and
487 $NO_2^-$ (r = 0.81), which might be due to the efficient heterogeneous conversion of $NO_2$ to $NO_2^-$
488 on mineral surface as explained, which is also supported by the highest concentration of $Ca^{2+}$ in
489 spring of HMB. High correlation between $Cl^-$ and $NO_3^-$ (r = 0.84) suggested their common
490 sources such as coal combustion and waste incineration (Pei et al., 2016).

491 In summer, no tight correlations were found among these ions in Ningbo and Lin'an, apart
492 from SNA. While in summer of Hangzhou (Table S15), in addition to that, $K^+$ correlated very
493 well with $Cl^-$ (r = 0.90) and $SO_4^{2-}$ (r = 0.88), and $Cl^-$ also correlated well with $NO_3^-$ (r = 0.83) and
494 $SO_4^{2-}$ (r = 0.80), indicating they may share part of the combustion related sources including fossil
495 fuel combustion, waste incineration and biomass burning, etc.

496 In autumn in this region, $K^+$ is found to correlate very well with $PM_{2.5}$, $NO_3^-$ and $NH_4^+$ at all
497 sampling sites (r > 0.80) (Table S4, S8, S12, S16). As discussed above, in this season these
498 components could be affected heavily by agricultural activities (livestock waste volatilization
499 and nitrogen containing fertilizer) as well as land clearing practice. Besides, high correlations of
500 $Na^+$ and $Cl^-$ (r = 0.80), $Ca^{2+}$ and $NO_2^-$ (0.88) were observed in HMB (Table S16). $Na^+$ is also
501 found to correlate well with $NO_2^-$ (r = 0.87) at UNNC (Table S4), and $K^+$ is found to correlate
502 with both primary $Ca^{2+}$ (r = 0.80) and secondary $SO_4^{2-}$ (r = 0.87) in NMB (Table S8), possibly

503 due to the similar transport pathways of air masses or mixture of both primary and secondary
504 aerosols (Xu et al., 2014).

505 3.4.3. Chemical conversions of species– sulfur and nitrogen oxidation ratios

506 The oxidation of $SO_2$ – $SO_4^{2-}$ and $NO_2$ – $NO_3^-$ has two mechanisms: homogeneous and
507 heterogeneous reactions (Liu et al., 2016). The former involves gas-phase $SO_2$ and $NO_2$
508 oxidation reactions with OH• radical; the latter for $SO_2$ – $SO_4^{2-}$ transformation includes $H_2O_2/O_3$
509 oxidation or metal catalyzed sulfur and in-cloud process, closely associated with RH and aerosol
510 mass concentration (Wang et al., 2006), and heterogeneous reactions for $NO_2$ – $NO_3^-$ is the
511 hydrolysis of $N_2O_5$ on pre-existing particulate matter, such as sulfate aerosols (Meng et al., 2016;
512 Zhang et al., 1995). Therefore, to investigate the conversion of above species in this study, sulfur
513 oxidation ratio (SOR) and nitrogen oxidation ratio (Xie et al.) were applied and they are
514 caculated as follows (Lin, 2002):

515 $$SOR = [nss\text{-}SO_4^{2-}]/([nss\text{-}SO_4^{2-}] + [SO_2]) \quad (8)$$

516 $$NOR = [NO_3^-]/([NO_3^-] + [NO_2]) \quad (9)$$

517 Where [nss-$SO_4^{2-}$], [$SO_2$], [$NO_3^-$] and [$NO_2$] represent their respective molar concentrations;
518 higher SOR and NOR indicate greater oxidation of $SO_2$ and $NO_2$, and more secondary aerosols
519 would be produced. The seasonal averaged $SO_2$, $NO_2$, $O_3$ concentrations and SOR, NOR values
520 at four sampling sites during the sampling campaign are presented in Supplemental Table S17.

521 It has been reported the photochemical oxidation of $SO_2$ to $SO_4^{2-}$ could occur when
522 SOR >0.1 (Ohta and Okita, 1990). The SOR values of all seasons at the 4 sampling sites were
523 above 0.1, indicating the oxidation of $SO_2$ occurred throughout the whole sampling campaign in
524 NZP. In four seasons, summer was observed with the highest SOR values at all sampling sites,
525 suggesting a considerable conversion of $SO_2$ to sulfate. As the homogeneous reaction of $SO_2$ and

526 OH• radical is a strong function of solar irradiation and ambient temperature (Meng et al., 2016),
527 homogeneous transition of $SO_2$ – $SO_4^{2-}$ may have contributed to the highest SOR in hot summer.
528 High presence of $O_3$ in summer may have also helped the oxidation of $SO_2$ (Meng et al., 2016).
529 Additionally, more efficient heterogeneous aqueous reaction of $SO_2$ and $NO_2$ could also occur
530 under high RH in summer to generate sulfate and gas-phase HONO significantly (Wang et al.,
531 2016a). It is noteworthy that the highest SOR value and lowest $SO_2$ concnetration were observed
532 simultaneously during the summer at all sites in NZP, very possibily due to 1) strong oxidation
533 of $SO_2$ to $SO_4^{2-}$; 2) the highest precipitation rate favorable for the efficient scavenging of $SO_2$
534 and 3) high PBL height during the summer beneficial to dispersion of $SO_2$. The SOR in other
535 seasons ranked as autumn > spring > winter. Lowest SOR in highly polluted winter could be
536 caused by: 1) the intensive emission of $SO_2$ from enhanced coal combustion, which was inclined
537 to be accumulated greatly under stagnant weather condition during cold winter with poor air
538 dispersion and circulation; 2) under stagnant weather, low solar radiation reduced the
539 photochemical activity which could not provide sufficient oxidants and hindered the
540 homogeneous reaction of $SO_2$ – $SO_4^{2-}$ (Hua et al., 2008; Liu et al., 2016); 3) lowest RH reduced
541 the possibility of heterogeneous aqueous reaction of $SO_2$ – $SO_4^{2-}$ , and eventually caused the
542 lowest SOR value in winter.

543 The NOR values in UNNC, LRABS and HMB shared a simlar seasonal pattern: Winter >
544 Spring > Autumn > Summer. The NOR values in highly-polluted winter and less polluted
545 summer are consistent with those reported in Shanghai, where the NOR during hazy days and
546 clean days were 0.18 and 0.08, respectively (Hua et al., 2015). As discussed, the seasonal
547 variation of nitrate has shown an inverse relationship with the seasonal mean air temperature
548 variations. Low temperature (< 15°C) could favor the transformation of gaseous $NO_2$ to

549 particulate $NO_3^-$ (Squizzato et al., 2012; US EPA, 1999). NOR in winter at these sampling sites
550 have shown the highest value (> 0.1), which implies the greatest oxidation degree of $NO_2$ to
551 $NO_3^-$ occured in the coldest season.. This is opposite to SOR trend, which shows the highest
552 during summer. As mentioned earlier, high RH can increase the possibility of heterogeneous
553 aqueous reaction of $SO_2$ and $NO_2$ to generate sulfate and gas-phase HONO, while less $NO_2$
554 might be converted into gas-phase HONO and more converted to particulate nitrate during the
555 dry winter. Also, lowest NOR in summer could be the result of the highest temperature in this
556 season favorable for the volatilization of nitrate when temperature > 30°C (Deng et al., 2015).
557 The NOR pattern in NMB showed slightly different from the other sites: Autumn (0.12) >
558 Winter (0.10) > Spring (0.07) > Summer (0.04). The highest NOR in autumn here might be
559 attibuted to the greater increase of $NO_3^-$ concentration (10.28 μg $m^{-3}$, in Table 3).

560 3.4.4. Principal component analysis

561 In order to investigate the possible sources of these ionic species in NZP, principal
562 component analysis (PCA, SPSS version 19.0, IBM Corp.) has been applied in this work and the
563 result is presented in Table 4. During the analysis, Varimax rotation was chosen to give a clearer
564 pattern of variables loading in factors, and this feature can make the loadings of obvious
565 variables close to 1 and non-obvious variables close to 0 (Meng et al., 2016). However, only
566 those loadings > 0.3 are shown in Table 4, and those variables with loading > 0.5 are considered
567 to be the indicators of the factors (Callén et al., 2009).

568 Nine ions ($Na^+$, $NH_4^+$, $K^+$, $Mg^{2+}$, $Ca^{2+}$, $Cl^-$, $NO_2^-$, $NO_3^-$, $SO_4^{2-}$) in NZP were selected for PCA
569 analysis. $Li^+$, $F^-$ and $PO_4^{3-}$ were undetectable in most of the aerosol samples due to their low
570 presence level in the atmosphere; therefore, they were not included in PCA analysis.

In winter, the variables resulted in 3 sources of eigenvalue > 1 and they explained 72.9% of variance in total. Factor 1 (Component 1) covered 42.8% of total variance, and is heavily loaded with $NH_4^+$, $K^+$, $Cl^-$, $NO_3^-$, $SO_4^{2-}$, suggesting the contributions from secondary inorganic aerosols, coal combustion and biomass burning. Factor 2, explaining 17.1% of the data variance, is loaded with $Na^+$, $Ca^{2+}$ and $Cl^-$, possibly indicating their marine and dust sources, along with coal combustion as well as factor 1. Factor 3 is responsible for 13.0% of the variance, mainly affected by $Mg^{2+}$ and $NO_2^-$. Since $NO_2$ on wet crustal particle surface can form $NO_2^-$ through heterogeneous reaction (Wang et al., 2015b) and crustal originated $Mg^{2+}$ ($r = 0.80$) and $Ca^{2+}$ ($r = 0.88$) were also found correlated well with $NO_2^-$ during winter at UNNC, therefore, $Mg^{2+}$ and $NO_2^-$ loaded factor 3 could be the result of heterogeneous conversion of $NO_2$.

In spring, 2 factors were obtained from PCA model. Factor 1, explaining 37.6% of variables, is loaded with $Na^+$, $NH_4^+$, $K^+$, $NO_3^-$ and $SO_4^{2-}$, indicating likely sources from sea salts, biomass burning and secondary aerosols. Factor 2 explains 18.6% of the variables, is affected by $Mg^{2+}$, $Ca^{2+}$ and $Cl^-$, suggesting the contributions of suspending dust and coal combustion to the fine particles in the atmosphere.

The PCA results in summer also have 2 factors, similar with those in spring. Factor 1, accounting for 38.6% of the variables, is loaded with $NH_4^+$, $K^+$, $Cl^-$, $NO_3^-$, $SO_4^{2-}$, suggesting contributions from industrial emissions, biomass burning and coal burning. Factor 2 explains 20.0% of the variance with loading of $Na^+$, $Mg^{2+}$ and $Ca^{2+}$, which are likely from sea salts and dust particles. This is consistent with the cluster results in Fig. 2 that most of the air masses were originated from the ocean, passed through mainland to reach studied sites and 10-29% was from central China. Therefore, the aerosols were characterized with both oceanic and terrestrial properties.

In autumn, 3 PCA factors were calculated, explaining 75.0% of the total variance. Factor 1 explained 44.5% of the variance, dominated by $NH_4^+$, $K^+$, $NO_3^-$ and $SO_4^{2-}$ with obvious loading above 0.8, and $K^+$ is found to correlate very well with $PM_{2.5}$, $NO_3^-$ and $NH_4^+$ at this region ($r > 0.80$), strongly suggesting emissions from industrial areas and biomass burning. Factor 2, responsible for 16.2% of the total variance, is loaded with $Na^+$, $Mg^{2+}$, $Ca^{2+}$ and $Cl^-$, indicating sources like sea salt, dust particles and coal burning. Only $NO_2^-$ in Factor 3 has loading above 0.5, indicating the origin from vehicle exhaust.

## 4. Conclusions

The seasonal variations of ion chemistry and sources of WSII were studied through a one-year sampling campaign at 4 representative sites in both Hangzhou and Ningbo of NZP. The annual averaged $PM_{2.5}$ and total WSII concentrations in NZP were 66.2 ± 37.7 μg $m^{-3}$ and 29.1 ± 19.9 μg $m^{-3}$, respectively. WSII in this region were dominated by $SO_4^{2-}$, $NO_3^-$, $NH_4^+$, $Cl^-$ and $K^+$. SNA ranked as the top three ions, accounting for 88.0% of total WSII and 38.7% of $PM_{2.5}$ occurrence levels. The seasonal average WSII exhibited the highest in winter and lowest in summer and spatially the annual total WSII at sites in Ningbo were relatively lower than those in Hangzhou, indicating the aerosol ionic pollution was more severe within the provincial capital municipality.

Aerosol acidity was also studied through ion balance. At UNNC and HMB, $NO_3^-$ and $SO_4^{2-}$ were mostly neutralized by $Ca^{2+}$ and $NH_4^+$. In winter and spring at LRABS, the alkaline nature of aerosols could be possibly due to the increased biomass burning emission and volatilization of ammonia containing fertilizer; but the alkaline nature of aerosol in NMB could be the result of enhanced traffic emitted $NH_3$. Among all cations, $NH_4^+$ was the predominant neutralizing ion

with the highest neutralization factor (NF); while the NFs of nss-$Ca^{2+}$, nss-$K^+$ and $Mg^{2+}$ were lower than 0.2, implying minor impact of these ions in the neutralization of aerosol acidity.

High ratios of nss-$SO_4^{2-}/SO_4^{2-}$, nss-$K^+/K^+$ and nss-$Ca^{2+}/Ca^{2+}$ at all four sites of NZP indicated minor marine contribution to these ions. High correlations of $NH_4^+$ with $NO_3^-$ and $SO_4^{2-}$ (r: 0.8~1.0) were observed throughout the sampling period at 4 sites and the annual averaged molar ratio of $[NH_4^+]/[SO_4^{2-}]$ of 4 sites were all above 3.3, indicating $NH_4^+$ existed predominantly as ammonium sulfates, ammonium bi-sulfates and ammonium nitrates in aerosols. The SOR value in all seasons of NZP were above 0.1, indicating $SO_2$ – $SO_4^{2-}$ transformation dominantly occurred throughout the year in NZP, and it was the highest in summer and lowest in winter; however, the NOR seasonal pattern was the opposite to that of SOR. The seasonal values of SOR and NOR seem to be significantly affected by both homogeneous and heterogeneous reactions for the gaseous precursors converted to secondary ions and volatilization of nitrates under high ambient temperature.

The sources of WSII were also investigated by PCA and the results showed that they were predominantly from industrial emissions, biomass burning, secondary inorganic aerosols, moderately from dust and soil originated particles and minorly from sea salts. In addition, the air mass backward trajectory analysis also showed that the contribution from transboundary transport of aerosols from highly polluted north China may not be negligible.

**Acknowledgement**

This work was carried out at the International Doctoral Innovation Centre (IDIC). The authors acknowledge the financial support from the International Doctoral Innovation Centre, Ningbo Education Bureau, Ningbo Science and Technology Bureau, China's MOST and The University of Nottingham. This work is also partially supported by Natural Science Foundation

639 of China (41303091, 41405116, 41675124 & 91544229), EPSRC grant EP/L016362/1, Zhejiang
640 Provincial Applied Research Program for Commonweal Technology (2015C33011), Strategic
641 Priority Research Program (B) of the Chinese Academy of Sciences (XDB05020403), and Open
642 Funds from Jiangsu Key Laboratory of AEMPC (KHK1304 & KHK1204).

643 **Conflict of interests**

644 The authors declare no conflict of interests at personal and/or organizational level.

## Reference


Baek, B.H., Aneja, V.P., Tong, Q., 2004. Chemical coupling between ammonia, acid gases, and fine particles. Environ. Pollut. 129, 89-98.

Balasubramanian, R., Qian, W.B., Decesari, S., Facchini, M.C., Fuzzi, S., 2003. Comprehensive characterization of $PM_{2.5}$ aerosols in Singapore. J. Geophys. Res-Atmos. 108.

Behera, S.N., Cheng, J., Huang, X., Zhu, Q., Liu, P., Balasubramanian, R., 2015. Chemical composition and acidity of size-fractionated inorganic aerosols of 2013-14 winter haze in Shanghai and associated health risk of toxic elements. Atmos. Environ. 122, 259-271.

Callén, M.S., de la Cruz, M.T., López, J.M., Navarro, M.V., Mastral, A.M., 2009. Comparison of receptor models for source apportionment of the $PM_{10}$ in Zaragoza (Spain). Chemosphere 76, 1120-1129.

Chen, J., Li, C., Ristovski, Z., Milic, A., Gu, Y., Islam, M.S., Wan,g S., Hao, J., Zhang, H., He, C., Guo, H., Fu, H., Miljevic, B., Morawska, L., Thai, P., Lam, Y.F., Pereira, G., Ding, A., Huang, X., Dumka, U.C., 2016. A review of biomass burning: Emissions and impacts on air quality, health and climate in China. Sci. Total Environ.

Chow, J.C., Watson, J.G., Kuhns, H., Etyemezian, V., Lowenthal, D.H., Crow, D., Kohl, S.D., Engelbrecht, J.P., Green, M.C., 2004. Source profiles for industrial, mobile, and area sources in the Big Bend Regional Aerosol Visibility and Observational study. Chemosphere 54, 185-208.

Deng, X.L., Shi, C.E., Wu, B.-w., Yang, Y.J., Jin, Q., Wang, H.L., Zhu S., Yu C., 2016. Characteristics of the water-soluble components of aerosol particles in Hefei, China. J. Environ. Sci. 42, 32-40.

Draxler, R.R.R., G.D., 2013. HYSPLIT (HYbrid Single-Particle Lagrangian Integrated Trajectory) Model access via NOAA ARL READY Website (http://ready.arl.noaa.gov/HYSPLIT.php). NOAA Air Resources Laboratory, Silver Spring, MD.

Fang, G.C., Lin, S.C., Chang, S.Y., Lin, C.Y., Chou, C.C.K., Wu, Y.J., Chen, Y.C., Chen, W.T., Wu, T.L., 2011. Characteristics of major secondary ions in typical polluted atmospheric aerosols during autumn in central Taiwan. J. Environ. Manage. 92, 1520-1527.

Gao, X., Yang, L., Cheng, S., Gao, R., Zhou, Y., Xue, L., Shou, Y., Wang, J., Wang, X., Nie, W., Xu, P., Wang, W., 2011. Semi-continuous measurement of water-soluble ions in $PM_{2.5}$

676 in Jinan, China: Temporal variations and source apportionments. Atmos. Environ. 45, 6048-
677 6056.
678 Haas, J., Ban, Y.F., 2014. Urban growth and environmental impacts in Jing-Jin-Ji, the Yangtze,
679 River Delta and the Pearl River Delta. Int. J. Appl. Earth Obs. Geoinf. 30, 42-55.
680 Han, B., Zhang, R., Yang, W., Bai, Z., Ma, Z., Zhang, W., 2016. Heavy haze episodes in
681 Beijing during January 2013: Inorganic ion chemistry and source analysis using highly time-
682 resolved measurements from an urban site. Sci. Total Environ. 544, 319-329.
683 He, J., Balasubramanian, R., 2008. Rain-aerosol coupling in the tropical atmosphere of
684 Southeast Asia: distribution and scavenging ratios of major ionic species. J. Atmos. Chem.
685 60, 205-220.
686 He, J., Balasubramanian, R., Burger, D., Hicks, K., Kuylenstierna, J.C.I., Palani, S., 2011. Dry
687 and wet atmospheric deposition of nitrogen and phosphorus in Singapore. Atmos. Environ.
688 45, 2760-2768.
689 He, K.B., Yang, F.M., Ma, Y.L., Zhang, Q., Yao, X.H., Chan, C.K., Cadle, S., Chan, T.,
690 Mulawa, P., 2001. The characteristics of $PM_{2.5}$ in Beijing, China. Atmos. Environ. 35, 4959-
691 4970.
692 Hu, G., Zhang, Y., Sun, J., Zhang, L., Shen, X., Lin, W., Yang, Y., 2014. Variability, formation
693 and acidity of water-soluble ions in $PM_{2.5}$ in Beijing based on the semi-continuous
694 observations. Atmos. Res. 145–146, 1-11.
695 Hu, M., Wu, Z., Slanina, J., Lin, P., Liu, S., Zeng, L., 2008. Acidic gases, ammonia and water-
696 soluble ions in $PM_{2.5}$ at a coastal site in the Pearl River Delta, China. Atmos. Environ. 42,
697 6310-6320.
698 Hua, W., Chen, Z.M., Jie, C.Y., Kondo, Y., Hofzumahaus, A., Takegawa, N., Chang, C.C., Lu,
699 K.D., Miyazaki, Y., Kita, K., Wang, H.L., Zhang, Y.H., Hu, M., 2008. Atmospheric
700 hydrogen peroxide and organic hydroperoxides during PRIDE-PRD'06, China: their
701 concentration, formation mechanism and contribution to secondary aerosols. Atmos. Chem.
702 Phys. 8, 6755-6773.
703 Hua, Y., Cheng, Z., Wang, S., Jiang, J., Chen, D., Cai, S., Fu, X., Fu, Q., Chen, C., Xu, B., Yu,
704 J., 2015. Characteristics and source apportionment of $PM_{2.5}$ during a fall heavy haze episode
705 in the Yangtze River Delta of China. Atmos. Environ. 123, Part B, 380-391.

706 Huang, X., Liu, Z., Zhang, J., Wen, T., Ji, D., Wang, Y., 2016. Seasonal variation and
707 secondary formation of size-segregated aerosol water-soluble inorganic ions during
708 pollution episodes in Beijing. Atmos. Res. 168, 70-79.
709 Kang, C.M., Lee, H.S., Kang, B.W., Lee, S.K., Sunwoo, Y., 2004. Chemical characteristics of
710 acidic gas pollutants and $PM_{2.5}$ species during hazy episodes in Seoul, South Korea. Atmos.
711 Environ. 38, 4749-4760.
712 Kang, J., Cho, B.C., Lee, C.B., 2010. Atmospheric transport of water-soluble ions ($NO_3^-$, $NH_4^+$
713 and nss-$SO_4^{2-}$) to the southern East Sea (Sea of Japan). Sci. Total Environ. 408, 2369-2377.
714 Kong, S., Wen, B., Chen, K., Yin, Y., Li, L., Li, Q., Yuan, L., Li, X., Sun, X., 2014. Ion
715 chemistry for atmospheric size-segregated aerosol and depositions at an offshore site of
716 Yangtze River Delta region, China. Atmos. Res. 147–148, 205-226.
717 Li, B., Zhang, J., Zhao, Y., Yuan, S., Zhao, Q., Shen, G., Wu H., 2015. Seasonal variation of
718 urban carbonaceous aerosols in a typical city Nanjing in Yangtze River Delta, China.
719 Atmos. Environ. 106, 223-231.
720 Li, J.W., Han, Z.W., 2016. Seasonal Variation of Nitrate Concentration and Its Direct Radiative
721 Forcing over East Asia. Atmosphere 7.
722 Lin, C.C., Huang, K.L., Chen, S.J., Liu, S.C., Tsai, J.H., Lin, Y.C., Lin, W.Y., 2009. $NH_4^+$,
723 $NO_3^-$, and $SO_4^{2-}$ in roadside and rural size-resolved particles and transformation of
724 NO2/SO2 to nanoparticle-bound $NO_3^-$/$SO_4^{2-}$. Atmos. Environ. 43, 2731-2736.
725 Lin, J.J., 2002. Characterization of water-soluble ion species in urban ambient particles.
726 Environ. Int. 28, 55-61.
727 Liu, Z.R., Hu, B., Zhang, J.K., Yu, Y.C., Wang, Y.S., 2016. Characteristics of aerosol size
728 distributions and chemical compositions during wintertime pollution episodes in Beijing.
729 Atmos. Res. 168, 1-12.
730 Meng, C.C., Wang, L.T., Zhang, F.F., Wei, Z., Ma, S.M., Ma, X., Yang, J., 2016.
731 Characteristics of concentrations and water-soluble inorganic ions in $PM_{2.5}$ in Handan City,
732 Hebei province, China. Atmos. Res. 171, 133-146.
733 MEP, 2012. China National Ambient Air Quality Standards, Ministry of Environmental
734 Protection, Beijing, China.

Niu, X., Cao, J., Shen, Z., Ho, S.S.H., Tie, X., Zhao, S., Xu, H., Zhang, T., Huang, R., 2016. $PM_{2.5}$ from the Guanzhong Plain: Chemical composition and implications for emission reductions. Atmos. Environ. 147, 458-469.

Ohta, S., Okita, T., 1990. A chemical characterization of atmospheric aerosol in Sapporo. Atmos. Environ. Part A. General Topics. 24, 815-822.

Pan, Y.P., Tian, S.L., Liu, D.W., Fang, Y.T., Zhu, X.Y., Zhang, Q., Zheng, B., Michalski, G., Wang, Y.S., 2016. Fossil Fuel Combustion-Related Emissions Dominate Atmospheric Ammonia Sources during Severe Haze Episodes: Evidence from N-15-Stable Isotope in Size-Resolved Aerosol Ammonium. Environ. Sci. Technol. 50, 8049-8056.

Pathak, R.K., Wu, W.S., Wang, T., 2009. Summertime $PM_{2.5}$ ionic species in four major cities of China: nitrate formation in an ammonia-deficient atmosphere. Atmos. Chem. Phys. 9, 1711-1722.

Pei, B., Wang, X., Zhang, Y., Hu, M., Sun, Y., Deng, J., Dong, L., Fu, Q., Yan, N., 2016. Emissions and source profiles of $PM_{2.5}$ for coal-fired boilers in the Shanghai megacity, China. Atmos. Pollut. Res. 7, 577-584.

Pope, C.A., Dockery, D.W., 2006. Health effects of fine particulate air pollution: Lines that connect. J. Air Waste Manage. Assoc. 56, 709-742.

Pope, C.A., III Burnett, R.T., Thun, M.J., Calle, E.E., Krewski, D., Ito, K., Thurston, G.D., 2002. Lung cancer, cardiopulmonary mortality, and long-term exposure to fine particulate air pollution. J. Am. Med. Assoc. (JAMA) 287, 1132-1141.

Qiao, T., Zhao, M., Xiu, G., Yu, J., 2015. Seasonal variations of water soluble composition (WSOC, Hulis and WSIIs) in $PM_1$ and its implications on haze pollution in urban Shanghai, China. Atmos. Environ. 123, Part B, 306-314.

Ran, L., Deng, Z.Z., Wang, P.C., Xia, X.A., 2016. Black carbon and wavelength-dependent aerosol absorption in the North China Plain based on two-year aethalometer measurements. Atmos. Environ. 142, 132-144.

Rolph, G.D., 2013. Real-time Environmental Applications and Display sYstem (READY) Website (http://ready.arl.noaa.gov) NOAA Air Resources Laboratory, Silver Spring, MD.

Safai, P.D., Budhavant, K.B., Rao, P.S.P., Ali, K., Sinha, A., 2010. Source characterization for aerosol constituents and changing roles of calcium and ammonium aerosols in the neutralization of aerosol acidity at a semi-urban site in SW India. Atmos. Res. 98, 78-88.

766 Satsangi, A., Pachauri, T., Singla, V., Lakhani, A., Kumari, K.M., 2013. Water Soluble Ionic
767 Species in Atmospheric Aerosols: Concentrations and Sources at Agra in the Indo-Gangetic
768 Plain (IGP). Aerosol Air Qual. Res. 13, 1877-1889.
769 Seidel, D.J., Ao, C.O., Li, K., 2010. Estimating climatological planetary boundary layer heights
770 from radiosonde observations: Comparison of methods and uncertainty analysis. J.
771 Geophys. Res-Atmos. 115.
772 Sheng, L., Tang, X., You, H., Gu, Q., Hu, H., 2017. Comparison of the urban heat island
773 intensity quantified by using air temperature and Landsat land surface temperature in
774 Hangzhou, China. Ecol. Indic. 72, 738-746.
775 Squizzato, S., Masiol, M., Innocente, E., Pecorari, E., Rampazzo, G., Pavoni, B., 2012. A
776 procedure to assess local and long-range transport contributions to $PM_{2.5}$ and secondary
777 inorganic aerosol. J. Aerosol Sci. 46, 64-76.
778 Tao, J., Ho, K.F., Chen, L., Zhu, L., Han, J., Xu, Z., 2009. Effect of chemical composition of
779 $PM_{2.5}$ on visibility in Guangzhou, China, 2007 spring. Particuology 7, 68-75.
780 Tian, S., Pan, Y., Liu, Z., Wen, T., Wang, Y., 2014. Size-resolved aerosol chemical analysis of
781 extreme haze pollution events during early 2013 in urban Beijing, China. J. Hazard. Mater.
782 279, 452-460.
783 Toledano, C., Cachorro, V.E., Gausa, M., Stebel, K., Aaltonen, V., Berjón, A., Ortiz de
784 Galisteo, J.P., de Frutos, A.M., Bennouna, Y., Blindheim, S., Myhre, C.L., Zibordi, G.,
785 Wehrli, C., Kratzer, S., Hakansson, B., Carlund, T., de Leeuw, G., Herber, A., Torres, B.,
786 2012. Overview of sun photometer measurements of aerosol properties in Scandinavia and
787 Svalbard. Atmos. Environ. 52, 18-28.
788 Tsai, Y.I., Chen, C.L., 2006. Atmospheric aerosol composition and source apportionments to
789 aerosol in southern Taiwan. Atmos. Environ. 40, 4751-4763.
790 Ueda, S., Hirose, Y., Miura, K., Okochi, H., 2014. Individual aerosol particles in and below
791 clouds along a Mt. Fuji slope: Modification of sea-salt-containing particles by in-cloud
792 processing. Atmos. Res. 137, 216-227.
793 US EPA, 1999. Particulate matter ($PM_{2.5}$) speciation guidance document (Third draft). 69.
794 Waldman, J.M., Lioy, P.J., Zelenka, M., Jing, L., Lin, Y.N., He, Q.C., Qian, Z.M., Chapman,
795 R., Wilson, W.E., 1991. Wintertime measurements of aerosol acidity and trace elements in
796 Wuhan, a city in central China. Atmos. Environ. Part B. Urban Atmosphere 25, 113-120.

Wang, G., Zhang, R., Gomez, M.E., Yang, L., Levy, Zamora, M., Hu, M., Lin, Y., Peng, J., Guo, S., Meng, J., Li, J., Cheng, C., Hu, T., Ren, Y., Wang, Y., Gao, J., Cao, J., An, Z., Zhou, W., Li, G., Wang, J., Tian, P., Marrero-Ortiz, W., Secrest, J., Du, Z., Zheng, J., Shang, D., Zeng, L., Shao, M., Wang, W., Huang, Y., Wang, Y., Zhu, Y., Li, Y., Hu, J., Pan, B., Cai, L., Cheng, Y., Ji, Y., Zhang, F., Rosenfeld, D., Liss, P.S., Duce, R.A., Kolb, C.E., Molina, M.J., 2016a. Persistent sulfate formation from London Fog to Chinese haze. Proc. Natl. Acad. Sci. U. S. A. 113, 13630-13635.

Wang, H., An, J., Cheng, M., Shen, L., Zhu, B., Li, Y., Wang, Y., Duan, Q., Sullivan, A., Xia, L., 2016b. One year online measurements of water-soluble ions at the industrially polluted town of Nanjing, China: Sources, seasonal and diurnal variations. Chemosphere 148, 526-536.

Wang, H., Zhu, B., Shen, L., Xu, H., An, J., Xue, G., Cao, J., 2015a. Water-soluble ions in atmospheric aerosols measured in five sites in the Yangtze River Delta, China: Size-fractionated, seasonal variations and sources. Atmos. Environ. 123, Part B, 370-379.

Wang, H.L., Qiao, L.P., Lou, S.R., Zhou, M., Ding, A.J., Huang, H.Y., Chen, J.M., Wang, Q., Tao, S.K., Chen, C.H., Li, L., Huang, C., 2016c. Chemical composition of $PM_{2.5}$ and meteorological impact among three years in urban Shanghai, China. J. Clean. Prod. 112, Part 2, 1302-1311.

Wang, L.W., Wen, L., Xu, C.H., Chen, J.M., Wang, X.F., Yang, L.X., Wang, W.X., Yang, X., Sui, X., Yao, L., Zhang, Q.Z., 2015b. HONO and its potential source particulate nitrite at an urban site in North China during the cold season. Sci. Total Environ. 538, 93-101.

Wang, Y., Ying, Q., Hu, J., Zhang, H., 2014. Spatial and temporal variations of six criteria air pollutants in 31 provincial capital cities in China during 2013–2014. Environ. Int. 73, 413-422.

Wang, Y., Zhuang, G., Zhang, X., Huang, K., Xu, C., Tang, A., Chen, J., An, Z., 2006. The ion chemistry, seasonal cycle, and sources of $PM_{2.5}$ and TSP aerosol in Shanghai. Atmos. Environ. 40, 2935-2952.

Whitburn, S., Van Damme, M., Kaiser, J.W., van der Werf, G.R., Turquety, S., Hurtmans, D., Clarisse, L., Clerbaux, C., Coheur, P.F., 2015. Ammonia emissions in tropical biomass burning regions: Comparison between satellite-derived emissions and bottom-up fire inventories. Atmos. Environ. 121, 42-54.

828 Xie, R., Seip, H.M., Wibetoe, G., Nori, S., McLeod, C.W., 2006. Heavy coal combustion as the
829 dominant source of particulate pollution in Taiyuan, China, corroborated by high
830 concentrations of arsenic and selenium in PM10. Sci. Total Environ. 370, 409-415.
831 Xu, H., Pu, J., He, J., Liu, J., Qi, B., Du, R., 2016a. Characteristics of atmospheric compositions
832 in the background area of Yangtze River Delta during heavy air pollution episode. Adv.
833 Meteorol. Article Number:7240486.
834 Xu, J.S., Xu, H.H., Xiao, H., Tong, L., Snape, C.E., Wang, C.J., He, J., 2016b. Aerosol
835 composition and sources during high and low pollution periods in Ningbo, China. Atmos.
836 Res. 178–179, 559-569.
837 Xu, J., Wang, Z., Yu, G., Qin, X., Ren, J., Qin, D., 2014. Characteristics of water soluble ionic
838 species in fine particles from a high altitude site on the northern boundary of Tibetan
839 Plateau: Mixture of mineral dust and anthropogenic aerosol. Atmos. Res. 143, 43-56.
840 Xue, Y., Zhou, Z., Nie, T., Wang, K., Nie, L., Pan, T., Wu, X., Tian, H., Zhong, L., Li, J., Liu,
841 H., Liu, S., Shao, P., 2016. Trends of multiple air pollutants emissions from residential coal
842 combustion in Beijing and its implication on improving air quality for control measures.
843 Atmos. Environ. 142, 303-312.
844 Yin, S., Wang, X., Xiao, Y., Tani, H., Zhong, G., Sun, Z., 2017. Study on spatial distribution of
845 crop residue burning and $PM_{2.5}$ change in China. Environ. Pollut. 220, 204-221.
846 Zhang, R.Y., Leu, M.T., Keyser, L.F., 1995. Hydrolysis of $N_2O_5O$ and $CLONO_2$ on the
847 H2SO4/HNO3/H2O ternary solutions under stratospheric conditions. Geophys. Res. Lett. 22,
848 1493-1496.
849 Zhang, T., Cao, J.J., Tie, X.X., Shen, Z.X., Liu, S.X., Ding, H., Han, Y.M., Wang, G.H., Ho,
850 K.F., Qiang, J., Li, W.T., 2011. Water-soluble ions in atmospheric aerosols measured in
851 Xi'an, China: Seasonal variations and sources. Atmos. Res. 102, 110-119.
852 Zhao, J., Zhang, F., Xu, Y., Che,n J., 2011. Characterization of water-soluble inorganic ions in
853 size-segregated aerosols in coastal city, Xiamen. Atmos. Res. 99, 546-562.
854 Zhou, J., Xing, Z., Deng, J., Du, K., 2016. Characterizing and sourcing ambient $PM_{2.5}$ over key
855 emission regions in China I: Water-soluble ions and carbonaceous fractions. Atmos.
856 Environ. 135, 20-30.

857 **Figure captions**

858 **Fig. 1** Locations of sampling sites in NZP, China (NCP: North China Plain; NWC: Northwest
859 China; PRD: Pearl River Delta; YRD: Yangtze River Delta)

860 **Fig. 2** Clusters of air mass backward trajectories during each season in sampling sites of NZP

861 **Fig. 3** Plot of anion equivalents (AE) vs cation equivalents (CE) in four seasons of NZP

862 **Fig. 4** The neutralization factors of nss-$Ca^{2+}$, $Mg^{2+}$, nss-$K^{+}$ and $NH_4^{+}$ in $PM_{2.5}$ at 4 sites of NZP

863 **Fig. 5** Concentration of non-sea salts and their respective non-sea salt ionic fractions at sampling
864 sites of NZP

865

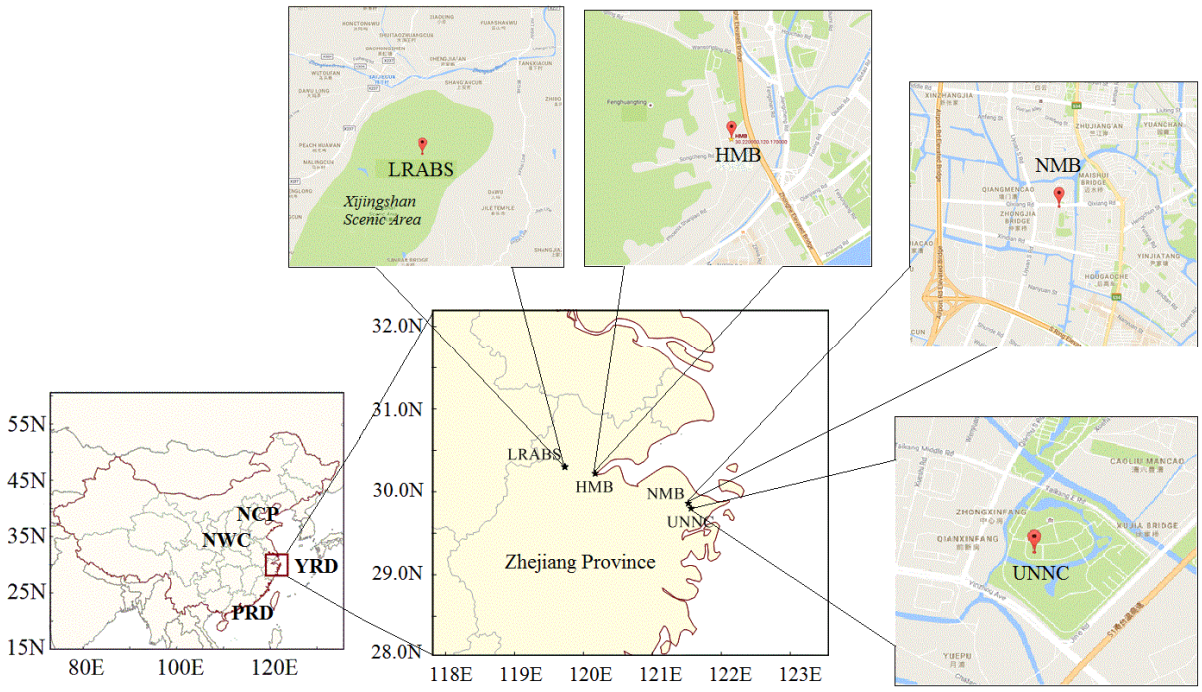


866

867 **Fig. 1.** Locations of sampling sites in NZP, China (NCP: North China Plain; NWC: Northwest China; PRD: Pearl
868 River Delta; YRD: Yangtze River Delta)

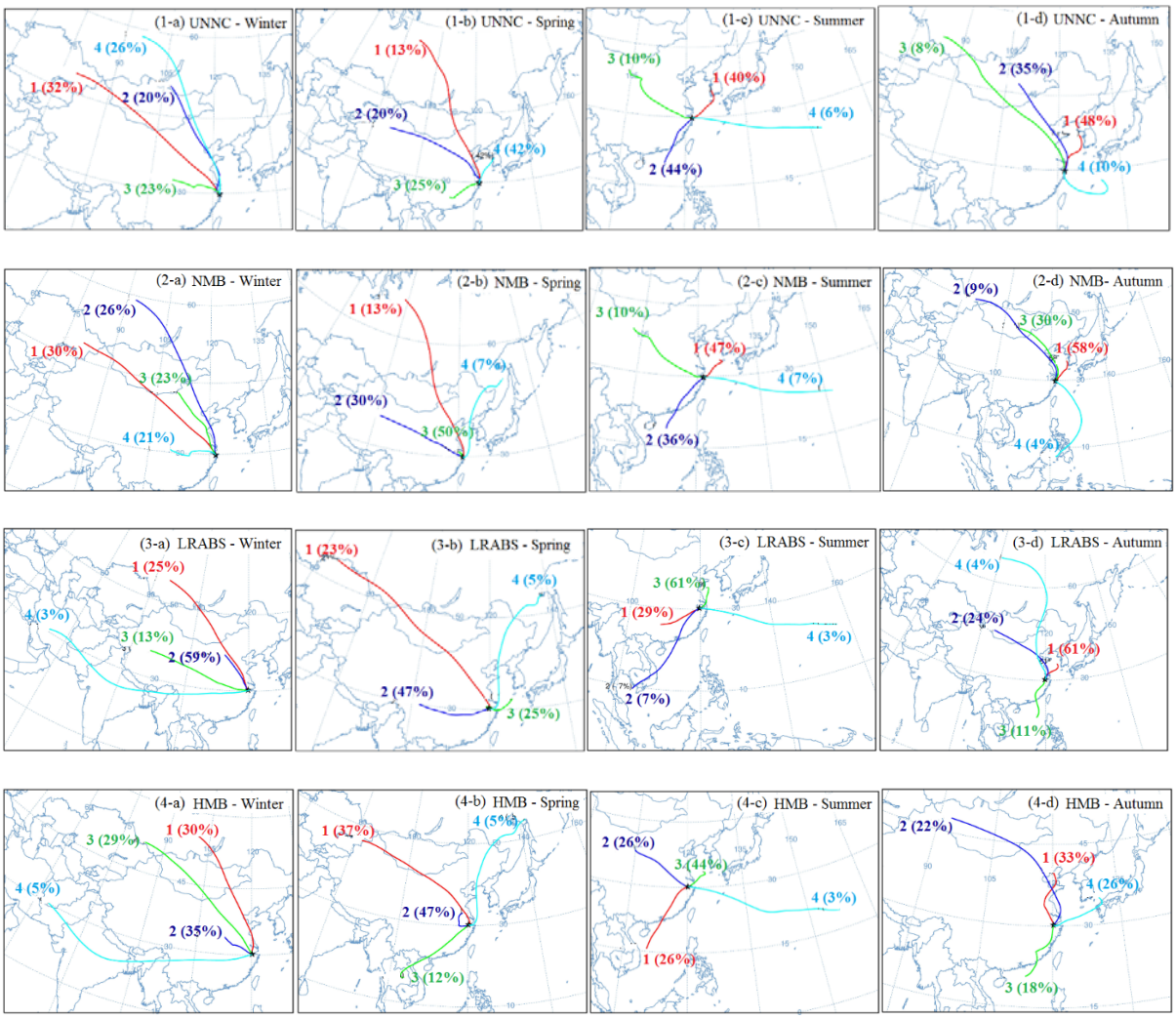


**Fig. 2.** Clusters of air mass backward trajectories during each season in sampling sites of NZP

875

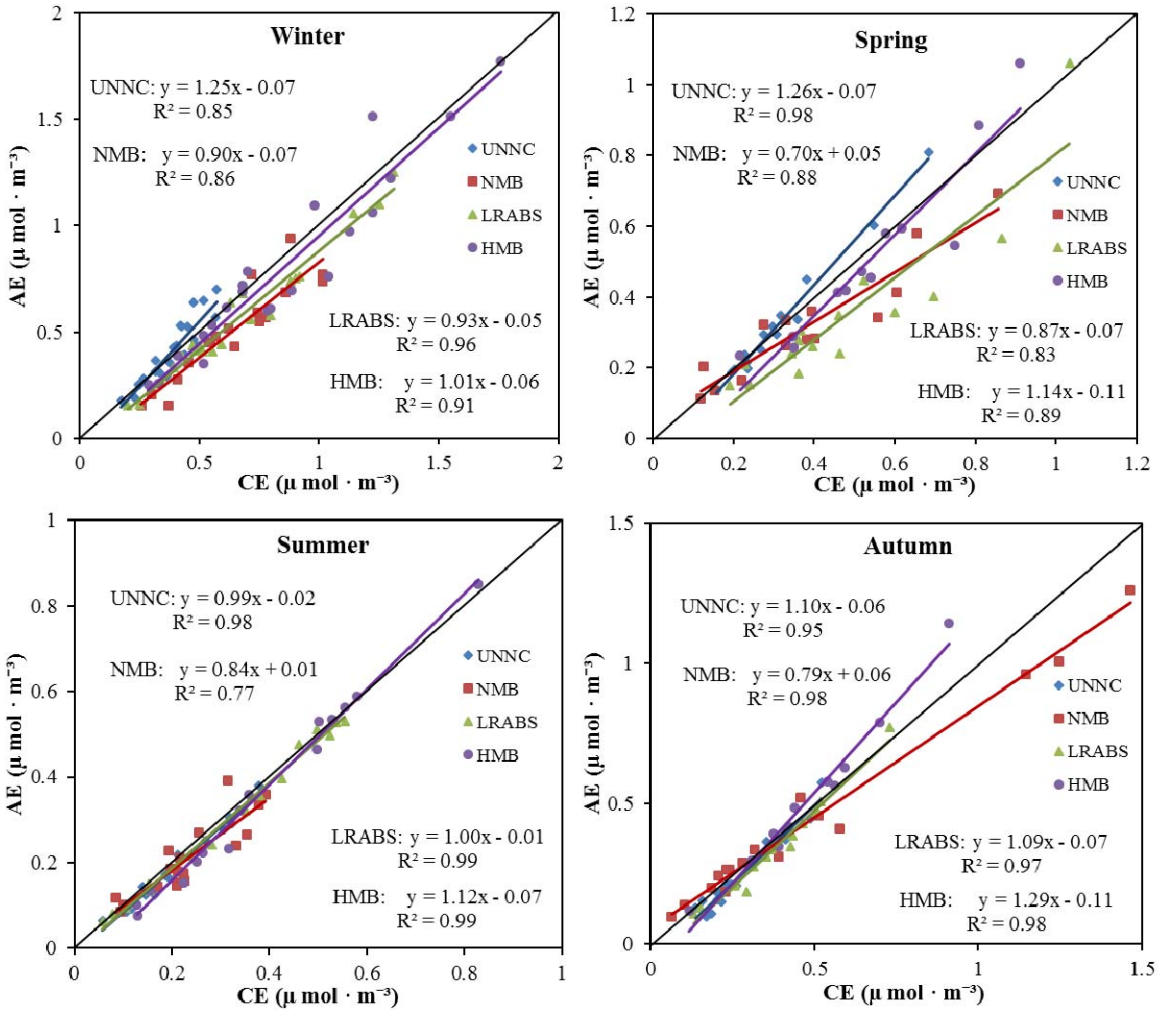


876

877 **Fig. 3.** Plot of anion equivalents (AE) vs cation equivalents (CE) in four seasons of NZP

878

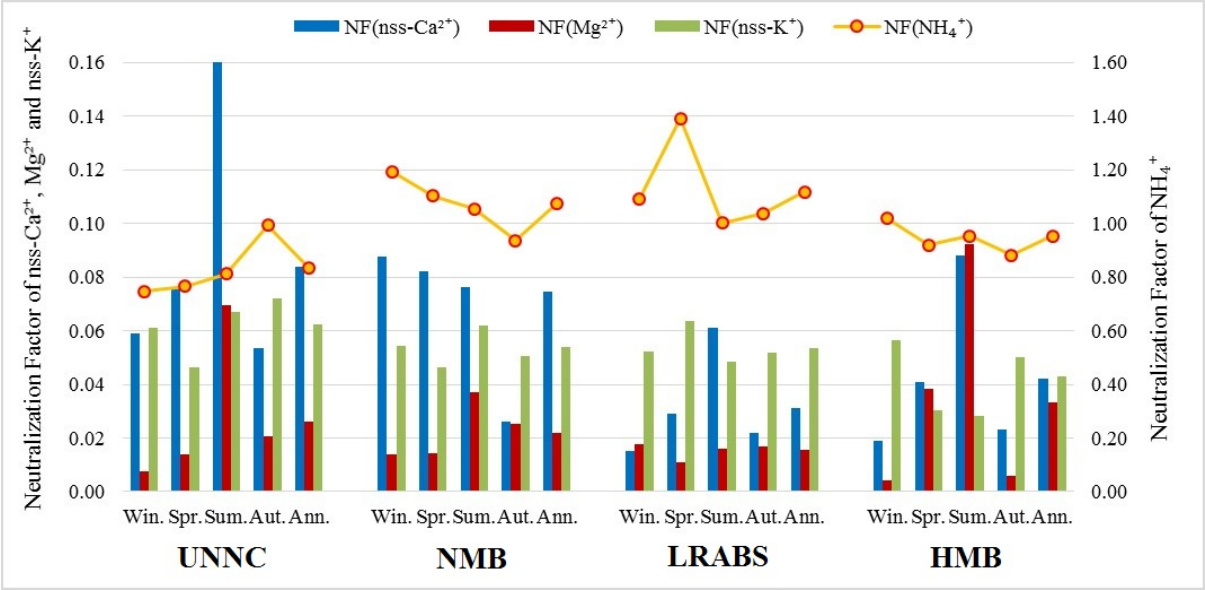


879

880 **Fig. 4.** The neutralization factors of nss-$Ca^{2+}$, $Mg^{2+}$, nss-$K^{+}$ and $NH_4^{+}$ in $PM_{2.5}$ at 4 sites of NZP

881

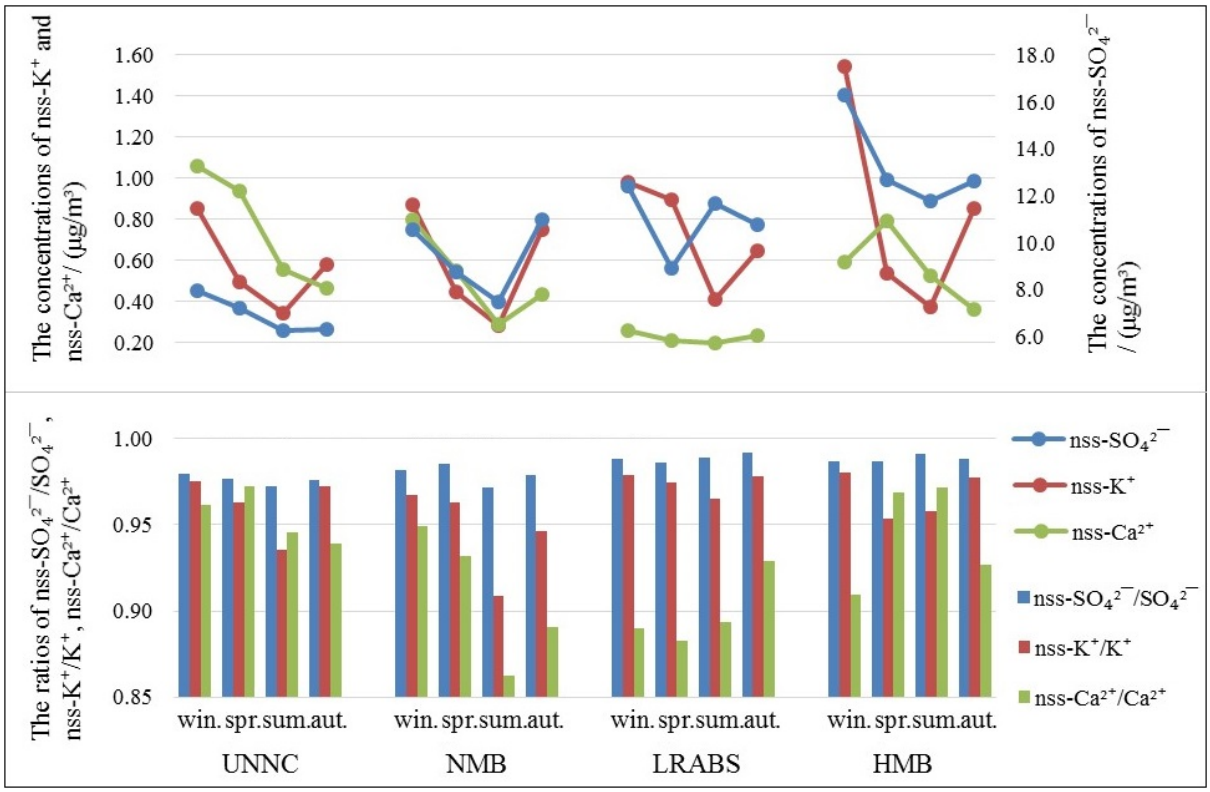


882

883 **Fig. 5.** Concentration of non-sea salts and their respective non-sea salt ionic fractions at sampling sites of NZP

884 **List of tables**

**Table 1**

Seasonal averaged $PM_{2.5}$ concentrations and meteorological data at four sampling sites during the 2014-2015 sampling campaign

| | | $PM_{2.5}$ concentrations ($\mu g\ m^{-3}$) | Wind Speed ($m\ s^{-1}$) | Precipitation (mm) | Temperature (°C) | Relative Humidity (%) |
|---|---|---|---|---|---|---|
| UNNC | Winter-2014 | 74.4 ± 30.3 | 2.4 | 0.052 | 6.5 | 64.2 |
| | Spring-2015 | 44.0 ± 17.4 | 2.4 | 0.052 | 15.6 | 76.1 |
| | Summer-2015 | 27.7 ± 8.5 | 2.4 | 0.110 | 26.5 | 80.1 |
| | Autumn-2015 | 50.1 ± 27.7 | 2.2 | 0.038 | 18.0 | 76.5 |
| | Annual average | 51.2 ± 29.1 | 2.3 | 0.063 | 16.6 | 74.2 |
| NMB | Winter-2014 | 98.1 ± 36.4 | 1.5 | 0.030 | 6.1 | 65.1 |
| | Spring-2015 | 79.3 ± 26.7 | 1.7 | 0.069 | 15.9 | 71.6 |
| | Summer-2015 | 33.6 ± 11.0 | 1.6 | 0.198 | 26.7 | 79.4 |
| | Autumn-2015 | 71.2 ± 47.5 | 1.4 | 0.166 | 18.2 | 77.6 |
| | Annual average | 70.4 ± 40.6 | 1.6 | 0.116 | 16.7 | 73.4 |
| LRABS | Winter-2014 | 93.7 ± 36.4 | 2.1 | 0.173 | 5.8 | 65.2 |
| | Spring-2015 | 59.0 ± 36.4 | 2.0 | 0.299 | 15.5 | 72.6 |
| | Summer-2015 | 42.6 ± 18.5 | 2.1 | 0.479 | 26.0 | 79.3 |
| | Autumn-2015 | 60.7 ± 29.7 | 1.8 | 0.221 | 17.2 | 77.9 |
| | Annual average | 66.3 ± 36.6 | 2.0 | 0.293 | 16.1 | 73.7 |
| HMB | Winter-2014 | 108.4 ± 44.2 | 2.1 | 0.014 | 6.9 | 62.1 |
| | Spring-2015 | 82.6 ± 24.5 | 2.2 | 0.051 | 15.8 | 64.1 |
| | Summer-2015 | 48.4 ± 17.6 | 2.1 | 0.165 | 27.7 | 72.5 |
| | Autumn-2015 | 68.0 ± 29.7 | 1.9 | 0.052 | 19.1 | 72.1 |
| | Annual average | 80.0 ± 39.6 | 2.1 | 0.070 | 17.4 | 67.7 |
| NZP* | Winter-2014 | 93.1 ± 38.4 | 2.0 | 0.067 | 6.3 | 64.1 |
| | Spring-2015 | 65.1 ± 30.9 | 2.1 | 0.118 | 15.7 | 71.1 |
| | Summer-2015 | 37.8 ± 16.2 | 2.0 | 0.238 | 26.7 | 77.8 |
| | Autumn-2015 | 61.3 ± 34.5 | 1.8 | 0.119 | 18.1 | 76.0 |
| | Annual average | 66.2 ± 37.7 | 2.0 | 0.136 | 16.7 | 72.3 |

NZP*: Data of NZP were calculated as the average values of those in four sampling sites of NZP

898 **Table 2**

899 Literature data of averaged $PM_{2.5}$, WSII, $SO_4^{2-}$, $NO_3^-$ and $NH_4^+$ concentrations in North China Plain (NCP), Northwest China (NWC), Pearl River Delta (PRD)
900 and Yangtze River Delta (YRD) of China

| Locations | Sampling period | Mass Concentrations (μg $m^{-3}$) | | | | | References |
|---|---|---|---|---|---|---|---|
| | | $PM_{2.5}$ | Total WSII (Total WSII/ $PM_{2.5}$) | $SO_4^{2-}$ | $NO_3^-$ | $NH_4^+$ | |
| Handan, NCP | 2013 – 2014 | 139.4 ± 98.5 | 63.1 ± 35.3 (45.3%) | 25.2 ± 13.5 | 20.6 ± 12.2 | 13.0 ± 8.1 | (Meng et al., 2016) |
| Hefei, NCP | 09/2012 – 11/2013 | 86.29 | 46.71 (54.1%) | 15.56 | 15.14 | 7.82 | (Deng et al., 2015) |
| Tianjin, NCP | 10/2012 – 08/2013 | 148.9 ± 91.1 | 64.2 (41%) | 24.2 ± 21.8 | 19.6 ± 16.5 | 8.5 ± 5.9 | (Zhou et al., 2016) |
| Xi'an, NWC | 03/2012 – 03/2013 | 169.3 ± 101.7 | 61.6 (36.4%) | 22.2 ± 16.8 | 17.1 ± 17.3 | 9.6 ± 8.7 | (Niu et al., 2016) |
| Weinan, NWC | 03/2012 – 03/2013 | 135.5 ± 70.0 | 60.2 (44.4%) | 24.7 ± 16.8 | 18.0 ± 17.5 | 10.0 ± 9.1 | (Niu et al., 2016) |
| Xi'an, NWC | 03/2006 – 03/2007 | 194.1 ± 78.6 | 76.5 (39.4%) | 35.6 ± 19.5 | 16.4 ± 10.1 | 11.4 ± 6.8 | (Zhang et al., 2011) |
| Guangzhou, PRD | 04/2007 | 79.2 ± 34.2 | 44.4 (55%) | 21.6 ± 10.7 | 9.5 ± 6.0 | 7.3 ± 3.9 | (Tao et al., 2009) |
| Zhongshan, PRD | 10/2012 – 08/2013 | 60.5 ± 46.5 | 22.4 (33%) | 9.8 ± 6.3 | 6.4 ± 7.7 | 2.8 ± 2.8 | (Zhou et al., 2016) |
| Shanghai, YRD | 01/2011 – 12/2013 | 47.0 ± 2.0 | 29.7 (63.2%) | 10.2 ± 0.6 | 9.2 ± 1.1 | 6.0 ± 0.7 | (Wang et al., 2016c) |
| Haining, YRD | 10/2012 – 08/2013 | 109.6 ± 59.4 | 42.0 (37%) | 16.5 ± 9.9 | 13.9 ± 12.0 | 6.1 ± 4.3 | (Zhou et al., 2016) |
| UNNC, Ningbo, this study | 11/2014 – 11/2015 | 51.2 ± 29.1 | 21.0 ± 10.8 (44.1%) | 7.1 ± 3.8 | 6.5 ± 4.9 | 3.9 ± 2.0 | This study |
| NMB, Ningbo, this study | 11/2014 – 11/2015 | 70.4 ± 40.6 | 26.7 ± 18.8 (38.6%) | 9.6 ± 4.8 | 7.3 ± 8.3 | 6.6 ± 5.1 | This study |
| LRABS, Lin'an, this study | 11/2014 – 11/2015 | 66.3 ± 36.6 | 29.7 ± 18.2 (44.9%) | 11.2 ± 6.3 | 8.7 ± 8.5 | 7.3 ± 4.5 | This study |
| HMB, Hangzhou, this study | 11/2014 – 11/2015 | 80.0 ± 39.6 | 41.3 ± 25.5 (49.2%) | 13.8 ± 7.6 | 14.2 ± 11.3 | 9.1 ± 5.7 | This study |

**Table 3**

Seasonal and annual averaged WSII concentrations at four sampling sites during the 2014-2015 sampling campaign

| Ion concentrations (μg $m^{-3}$) | | $Li^+$ | $Na^+$ | $NH_4^+$ | $K^+$ | $Mg^{2+}$ | $Ca^{2+}$ | $F^-$ | $Cl^-$ | $NO_2^-$ | $NO_3^-$ | $PO_4^{3-}$ | $SO_4^{2-}$ | Sum of total WSII |
|---|---|---|---|---|---|---|---|---|---|---|---|---|---|---|
| UNNC | Winter-2014 | 0.0 ± 0.0 | 0.5 ± 0.1 | 5.0 ± 1.8 | 0.9 ± 0.3 | 0.1 ± 0.0 | 1.1 ± 1.1 | 0.1 ± 0.1 | 2.5 ± 1.6 | 0.0 ± 0.0 | 10.6 ± 5.2 | 0.0 ± 0.0 | 8.1 ± 4.1 | 28.9 ± 9.7 |
| | Spring-2015 | 0.0 ± 0.0 | 0.5 ± 0.3 | 4.0 ± 2.0 | 0.5 ± 0.3 | 0.1 ± 0.1 | 0.9 ± 0.7 | 0.1 ± 0.1 | 2.2 ± 3.2 | 0.1 ± 0.1 | 6.6 ± 3.4 | 0.0 ± 0.0 | 7.4 ± 4.1 | 22.3 ± 11.0 |
| | Summer-2015 | 0.0 ± 0.0 | 0.5 ± 0.2 | 2.4 ± 1.4 | 0.4 ± 0.1 | 0.1 ± 0.1 | 0.5 ± 0.4 | 0.0 ± 0.0 | 0.4 ± 0.7 | 0.1 ± 0.1 | 2.3 ± 1.3 | 0.0 ± 0.0 | 6.4 ± 3.4 | 13.0 ± 6.2 |
| | Autumn-2015 | 0.0 ± 0.0 | 0.4 ± 0.1 | 3.8 ± 1.7 | 0.6 ± 0.3 | 0.1 ± 0.1 | 0.5 ± 0.4 | 0.0 ± 0.0 | 0.8 ± 0.9 | 0.0 ± 0.0 | 5.4 ± 3.9 | 0.0 ± 0.0 | 6.4 ± 3.5 | 17.9 ± 8.7 |
| | Annual average | 0.0 ± 0.0 | 0.5 ± 0.2 | 3.9 ± 2.0 | 0.6 ± 0.3 | 0.1 ± 0.1 | 0.8 ± 0.8 | 0.0 ± 0.1 | 1.5 ± 2.0 | 0.0 ± 0.1 | 6.5 ± 4.9 | 0.0 ± 0.0 | 7.1 ± 3.8 | 21.0 ± 10.8 |
| NMB | Winter-2014 | 0.0 ± 0.0 | 0.7 ± 0.3 | 9.4 ± 4.4 | 0.9 ± 0.4 | 0.1 ± 0.0 | 0.8 ± 0.8 | 0.0 ± 0.0 | 3.5 ± 2.3 | 0.1 ± 0.2 | 10.3 ± 7.6 | 0.0 ± 0.0 | 10.7 ± 4.0 | 36.4 ± 16.3 |
| | Spring-2015 | 0.0 ± 0.0 | 0.4 ± 0.1 | 5.9 ± 3.8 | 0.5 ± 0.2 | 0.1 ± 0.0 | 0.5 ± 0.4 | 0.1 ± 0.4 | 0.9 ± 0.8 | 0.7 ± 0.7 | 5.5 ± 4.0 | 0.1 ± 0.4 | 8.8 ± 4.6 | 23.4 ± 12.4 |
| | Summer-2015 | 0.0 ± 0.0 | 0.7 ± 0.5 | 3.2 ± 1.8 | 0.3 ± 0.3 | 0.1 ± 0.0 | 0.2 ± 0.3 | 0.2 ± 0.5 | 0.3 ± 0.3 | 0.2 ± 0.3 | 1.7 ± 1.4 | 0.0 ± 0.0 | 7.6 ± 3.1 | 14.5 ± 5.7 |
| | Autumn-2015 | 0.0 ± 0.0 | 0.6 ± 0.2 | 7.5 ± 7.2 | 0.8 ± 0.7 | 0.0 ± 0.0 | 0.2 ± 0.4 | 0.0 ± 0.0 | 1.1 ± 0.9 | 0.3 ± 0.3 | 10.3 ± 12.4 | 0.0 ± 0.0 | 11.2 ± 6.7 | 32.0 ± 27.0 |
| | Annual average | 0.0 ± 0.0 | 0.6 ± 0.4 | 6.6 ± 5.1 | 0.6 ± 0.5 | 0.1 ± 0.0 | 0.4 ± 0.5 | 0.1 ± 0.3 | 1.5 ± 1.8 | 0.3 ± 0.4 | 7.0 ± 8.3 | 0.0 ± 0.2 | 9.6 ± 4.8 | 26.7 ± 18.8 |
| LRABS | Winter-2014 | 0.1 ± 0.1 | 0.5 ± 0.2 | 10.2 ± 5.6 | 1.0 ± 0.4 | 0.2 ± 0.2 | 0.3 ± 0.2 | 0.1 ± 0.1 | 1.3 ± 1.1 | 0.1 ± 0.1 | 15.2 ± 8.7 | 0.2 ± 0.1 | 12.5 ± 7.1 | 41.6 ± 20.9 |
| | Spring-2015 | 0.0 ± 0.1 | 0.4 ± 0.2 | 7.5 ± 3.9 | 0.9 ± 1.5 | 0.1 ± 0.1 | 0.2 ± 0.1 | 0.0 ± 0.1 | 0.5 ± 0.6 | 0.2 ± 0.1 | 8.5 ± 9.3 | 0.0 ± 0.1 | 9.0 ± 4.8 | 27.4 ± 17.4 |
| | Summer-2015 | 0.0 ± 0.0 | 0.3 ± 0.1 | 4.9 ± 3.2 | 0.4 ± 0.2 | 0.0 ± 0.0 | 0.2 ± 0.1 | 0.0 ± 0.0 | 0.2 ± 0.1 | 0.2 ± 0.2 | 2.4 ± 2.0 | 0.1 ± 0.2 | 11.8 ± 7.4 | 20.6 ± 12.5 |
| | Autumn-2015 | 0.0 ± 0.1 | 0.3 ± 0.1 | 5.9 ± 2.5 | 0.7 ± 0.3 | 0.1 ± 0.1 | 0.2 ± 0.2 | 0.0 ± 0.0 | 0.3 ± 0.3 | 0.1 ± 0.1 | 6.7 ± 5.3 | 0.0 ± 0.0 | 10.9 ± 4.7 | 25.1 ± 11.6 |
| | Annual average | 0.0 ± 0.1 | 0.4 ± 0.2 | 7.3 ± 4.5 | 0.8 ± 0.7 | 0.1 ± 0.1 | 0.2 ± 0.2 | 0.0 ± 0.1 | 0.6 ± 0.8 | 0.1 ± 0.1 | 8.7 ± 8.5 | 0.1 ± 0.2 | 11.2 ± 6.3 | 29.6 ± 18.2 |
| HMB | Winter-2014 | 0.0 ± 0.0 | 0.7 ± 0.3 | 13.5 ± 6.7 | 1.6 ± 0.7 | 0.1 ± 0.0 | 0.6 ± 0.5 | 0.2 ± 0.0 | 3.4 ± 2.3 | 0.0 ± 0.1 | 21.9 ± 12.6 | 0.1 ± 0.1 | 16.5 ± 9.6 | 58.5 ± 29.7 |
| | Spring-2015 | 0.0 ± 0.0 | 0.5 ± 0.2 | 7.7 ± 3.2 | 0.6 ± 0.3 | 0.5 ± 0.3 | 0.8 ± 0.4 | 0.0 ± 0.1 | 1.0 ± 0.8 | 0.2 ± 0.3 | 13.3 ± 8.1 | 0.0 ± 0.1 | 12.8 ± 6.1 | 37.6 ± 16.8 |
| | Summer-2015 | 0.0 ± 0.0 | 0.4 ± 0.3 | 5.5 ± 3.2 | 0.4 ± 0.3 | 0.2 ± 0.2 | 0.5 ± 0.5 | 0.0 ± 0.0 | 0.4 ± 0.5 | 0.1 ± 0.1 | 5.7 ± 5.8 | 0.0 ± 0.1 | 11.9 ± 6.2 | 25.2 ± 15.7 |
| | Autumn-2015 | 0.0 ± 0.0 | 0.4 ± 0.3 | 7.3 ± 3.3 | 0.9 ± 0.4 | 0.1 ± 0.0 | 0.4 ± 0.2 | 0.0 ± 0.0 | 0.9 ± 0.6 | 0.1 ± 0.1 | 12.3 ± 8.9 | 0.2 ± 0.3 | 12.7 ± 6.0 | 35.2 ± 18.0 |
| | Annual average | 0.0 ± 0.0 | 0.5 ± 0.3 | 9.1 ± 5.7 | 0.9 ± 0.7 | 0.2 ± 0.2 | 0.6 ± 0.4 | 0.1 ± 0.1 | 1.7 ± 1.9 | 0.1 ± 0.2 | 14.2 ± 11.3 | 0.1 ± 0.2 | 13.8 ± 7.6 | 41.3 ± 25.5 |

903 **Table 4**

904 Seasonal principal component analysis results for water-soluble inorganic ions in $PM_{2.5}$ of northern Zhejiang
905 Province

| Season | 2014-Winter | | | 2015-Spring | | 2015-Summer | | 2015-Autumn | | |
|---|---|---|---|---|---|---|---|---|---|---|
| | Component | | | Component | | Component | | Component | | |
| | 1 | 2 | 3 | 1 | 2 | 1 | 2 | 1 | 2 | 3 |
| $Na^+$ | **0.555** | **0.582** | | **0.687** | 0.337 | 0.342 | **0.642** | 0.413 | **0.571** | 0.490 |
| $NH_4^+$ | **0.931** | | | **0.806** | - | **0.835** | - | **0.957** | | |
| $K^+$ | **0.868** | | | **0.675** | | **0.820** | | **0.942** | | |
| $Mg^{2+}$ | | 0.377 | **0.744** | 0.438 | **0.505** | | **0.554** | | **0.695** | -0.348 |
| $Ca^{2+}$ | | **0.730** | | | **0.815** | 0.484 | **0.673** | 0.311 | **0.505** | -0.623 |
| $Cl^-$ | **0.558** | **0.507** | | 0.465 | **0.534** | **0.564** | 0.359 | 0.442 | **0.538** | 0.450 |
| $NO_2^-$ | | - | **0.725** | | | | | | | **0.533** |
| $NO_3^-$ | **0.891** | | | **0.910** | | **0.846** | | **0.949** | | |
| $SO_4^{2-}$ | **0.882** | | | **0.729** | | **0.840** | - | **0.848** | | |
| Initial eigenvalue | 3.856 | 1.539 | 1.168 | 3.383 | 1.670 | 3.473 | 1.799 | 4.002 | 1.456 | 1.295 |
| % of Variance explained | 42.848 | 17.098 | 12.973 | 37.590 | 18.553 | 38.588 | 19.984 | 44.463 | 16.175 | 14.387 |
| % of Cumulative variance | 42.848 | 59.946 | 72.919 | 37.590 | 56.143 | 38.588 | 58.571 | 44.463 | 60.637 | 75.024 |

906 *Blanks in table are value < 0.3*